Operando Monitoring and Deciphering the Structural Evolution in Oxygen Evolution Electrocatalysis

Zuo, Shouwei; Wu, Zhi-Peng; Zhang, Huabin; Lou, Xiong Wen (David)

Published in:
Advanced Energy Materials

Published: 24/02/2022

Document Version:
Final Published version, also known as Publisher's PDF, Publisher's Final version or Version of Record

Published version (DOI):
10.1002/aenm.202103383

Publication details:
Zuo, S., Wu, Z.-P., Zhang, H., & Lou, X. W. (2022). Operando Monitoring and Deciphering the Structural Evolution in Oxygen Evolution Electrocatalysis. *Advanced Energy Materials*, *12*(8), Article 2103383. https://doi.org/10.1002/aenm.202103383

ADVANCED ENERGY MATERIALS
www.advenergymat.de

Operando Monitoring and Deciphering the Structural Evolution in Oxygen Evolution Electrocatalysis

Shouwei Zuo, Zhi-Peng Wu, Huabin Zhang, and Xiong Wen (David) Lou**

The oxygen evolution reaction (OER) acts as the bottleneck of some crucial energy conversion and storage technologies involving water electrolysis, CO_2 electrolysis, and metal-air batteries, among others. The challenging sluggish reaction kinetics of the OER can be overcome via developing highly efficient electrocatalysts, which experience a dynamic structural evolution process during the reaction. However, the reaction mechanism of the structural transformation of electrocatalysts during the OER and the structure-activity correlation in understanding the real active sites remain elusive. Fortunately, operando characterizations offer a platform to study the structural evolution processes and the reaction mechanisms of OER electrocatalysts. In this review, using several in situ/operando techniques some recent advances are elaborated with emphases on tracking the structural evolution processes of electrocatalysts, recording the reaction intermediates during electrocatalysis, and building a link between the structure and activity/stability of electrocatalysts. Moreover, theoretical considerations are also discussed to assist operando characterization understanding. Finally, some perspectives are provided which are expected to be helpful to tackle the current challenges in operando monitoring and unraveling the reaction mechanisms of OER electrocatalysts.

1. Introduction

The successful and efficient utilizations of the renewable electric energy via converting it into chemical energy stored in the forms of chemical fuels and high-energy-density batteries will fulfill the future highly renewable power system, which allows a greater penetration of renewable energy into the chemical industry.[1–3] Representative effective approaches involve water electrolysis to produce hydrogen, CO_2 reduction to transform the greenhouse gas to value-added chemicals, and metal-air batteries with high energy densities, among others. All of these promising next generation energy vectors for the future carbon-free society involve the crucial oxygen evolution reaction (OER) with sluggish reaction kinetics, which is facing great challenges at the lack of cost-effective, catalytically active, and robust OER electrocatalysts.[4–7] Despite tremendous research efforts have been made on the design and fabrication of the OER electrocatalysts with fantastic structures and excellent performance, as well as some characterizations and understandings largely based on ex situ approaches, the reaction mechanisms of the OER process currently remain elusive due to the lack of operando studies.[8–10] More importantly, the structures and chemical properties of OER electrocatalysts often change during the anodic oxidation reaction, which makes the situation even worse and hence leads to complex and unsolved reaction mechanisms.[11–14] To tackle the aforementioned challenges, a range of recent research progresses have been made on demonstrating a number of operando techniques as powerful tools to unravel the nature of the structural evolution and the reaction mechanisms of OER electrocatalysts, which are beneficial for the rational designs of efficient electrocatalysts.[11,14–16]

Recently, a number of reviews and research articles focusing on high-performance OER electrocatalysts in varied structures have been published,[6,17–20] but few summaries have been made on operando characterizations of OER electrocatalysts especially from the perspectives of structural evolution of catalysts while integrating different techniques in one platform. In this review, we focus on monitoring and deciphering the OER electrocatalysts using a variety of cutting-edge operando techniques with a focal point on the structural evolution process and the structure-performance correlation during the electrocatalysis. We start with a brief introduction of some fundamental understandings and operando characterization approaches for the OER. Then we expand the main text by elaborating on the structural evolution evidence and reaction mechanism studies of OER electrocatalysts obtained from a number of operando characterization methods involving operando microscopy characterizations, X-ray-based operando techniques, operando optical spectroscopies, and mass spectroscopies. Furthermore,

S. W. Zuo, H. Zhang
KAUST Catalysis Center (KCC)
King Abdullah University of Science and Technology (KAUST)
Thuwal 23955-6900, Saudi Arabia
E-mail: huabin.zhang@kaust.edu.sa
Z.-P. Wu, X. W. Lou
School of Chemical and Biomedical Engineering
Nanyang Technological University
62 Nanyang Drive, Singapore 637459
E-mail: xwlou@ntu.edu.sg
The ORCID identification number(s) for the author(s) of this article can be found under https://doi.org/10.1002/aenm.202103383.

DOI: 10.1002/aenm.202103383

the theoretical considerations for the simulation process have also been emphasized for elaborating more effective computational models. The summary of the current advances in operando characterization results and the provided perspectives in this review are expected to provide more comprehensive understandings of OER electrocatalysts on the structural evolution process during electrocatalysis and the reaction mechanisms especially for the structure-performance relationship, and hence to offer rational guidelines for the design and fabrication of more efficient OER electrocatalysts toward the large-scale commercialization in the near future.

2. Fundamentals and Operando Techniques for OER

A minimum theoretical potential of 1.23 V versus reversible hydrogen electrode (versus RHE) is required for an ideal OER catalyst to drive the reaction from the thermodynamic viewpoint. The sluggish reaction kinetics of the OER originates from its four-electron transfer nature. Practical OER electrocatalysts usually show deviated bindings of the key intermediates (e.g., *OH, *O, and *OOH), are restricted by the scaling relationships, and need to overcome the involved reaction barriers for each deprotonation step, leading to additional overpotentials to drive the reaction.[6,21–23] It is encouraging that significant advances on OER electrocatalysts have been made in the past few decades, pushing the electrochemical overpotential of the OER electrocatalysts approaching to a commercially available range, that is, 200–400 mV, which are largely based on laboratory testing results.[5,13,24–26] Moreover, besides the state-of-the-art noble metal-based OER electrocatalysts (e.g., IrO_2 and RuO_2), cost-effective and catalytically-active non-noble metal-based OER electrocatalysts are emerging as alternatives with impressive catalytic performance.[6] However, it is well acknowledged in the community that either noble metal-based or non-noble metal-based OER electrocatalysts would experience inevitable but significant structural evolution processes during the harsh anodic oxidation reaction.[5,14,27] Over a long period of time in the past, the structural changes of OER electrocatalysts before and after reactions are largely probed by ex situ characterizations, which often fail to provide convincible results because of the almost non-existence of short-lived intermediates as well as the inevitable aging, contamination, and damage on the catalyst during the sample preparation and measurement processes. It has given birth to the time- and spatially-resolved operando characterization techniques, aiming at gaining real time information to understand how the catalytic reactions happen, which serves as the focal point of this review.

The word of operando is borrowed from Latin, which means "operating" or "working" since the collected characterization information comes from an "operating" catalyst while the catalytic performance has been simultaneously recorded, whereas in situ means "on site."[28] In other words, operando experiments can reflect the information of catalysts at the real working conditions in practical devices, while in situ measurements often need to design special devices/cells to mimic the real working conditions of the catalysts and to meet the requirements of different characterization approaches. Very often, operando experiments are monitoring the evolutions of experiments by adding additional time-resolved components. Recently, a number of in situ/operando characterization methods including transmission electron microscopy (TEM), X-ray absorption spectroscopy (XAS), X-ray photoelectron spectroscopy (XPS), X-ray diffraction (XRD), Raman spectroscopy, infrared (IR) spectroscopy, mass spectroscopy, on-line inductively coupled plasma mass spectrometry (ICP-MS) and some other methodologies have been developed to study OER electrocatalysts under realistic reaction conditions (**Figure 1**).[15,29–33] The operando-obtained information offers us valuable opportunities to get more precise, in-depth, and comprehensive evidences and insights into the dynamic structural evolution process, the catalyst surface and intermediate interactions at the solid-liquid interface, and further the reaction mechanisms on the structure-performance correlations as well as the reaction pathways aided by theoretical calculations. However, each in situ/operando characterization approach shows its pros and cons. To name a few, in situ TEM characterization offers a direct observation to grab the catalyst's structural change, but is suffering from challenges in the fabrication of the in situ cell and the electron beam damage;[34] operando XAS is sensitive to the local coordination structure and oxidation state of elements in the catalysts, but is a bulk sensitive technique and usually fails to specifically reflect the information of catalytic reactions occurring at the catalyst surface region;[30] operando XRD technique has been well-developed, but is often hard to detect the surface amorphous structure of the reconstructed OER electrocatalyst.[35] Considering the advantages and disadvantages of each operando technique, combining different operando characterization approaches together in one map will help construct a full picture of the reaction, which is one important current research frontier in the field.

It is thus necessary to give a summary of the in situ/operando characterizations of the OER electrocatalysts for the purpose to depict the panorama of the reaction mechanism studies and to build integrated operando techniques for future works. In the following sections, we will highlight some recent advances in the structural evolution of OER electrocatalysts using a variety of quasi-operando and operando techniques. The current development status, capabilities, and limitations of each in situ/operando characterization methodology are elaborated in detailed examples. Theoretical considerations are also involved to try to simulate the real reaction operating conditions and to assist the understandings of operando experiments. Finally, some constructive perspectives and possible solutions are provided to tackle the current challenges.

3. Microscopy Characterizations

The reconstruction phenomenon of catalysts during the electrocatalytic OER process is often directly reflected by morphology and phase structure changes, which can be observed by in situ or quasi-in situ microscopy techniques.[36–38] In situ microscopy characterizations, typically involving quasi-in situ identical location TEM[39] and in situ liquid cell TEM techniques, are developed for evaluating the solid-liquid electrochemical reactions such as OER and oxygen reduction reaction, among others.

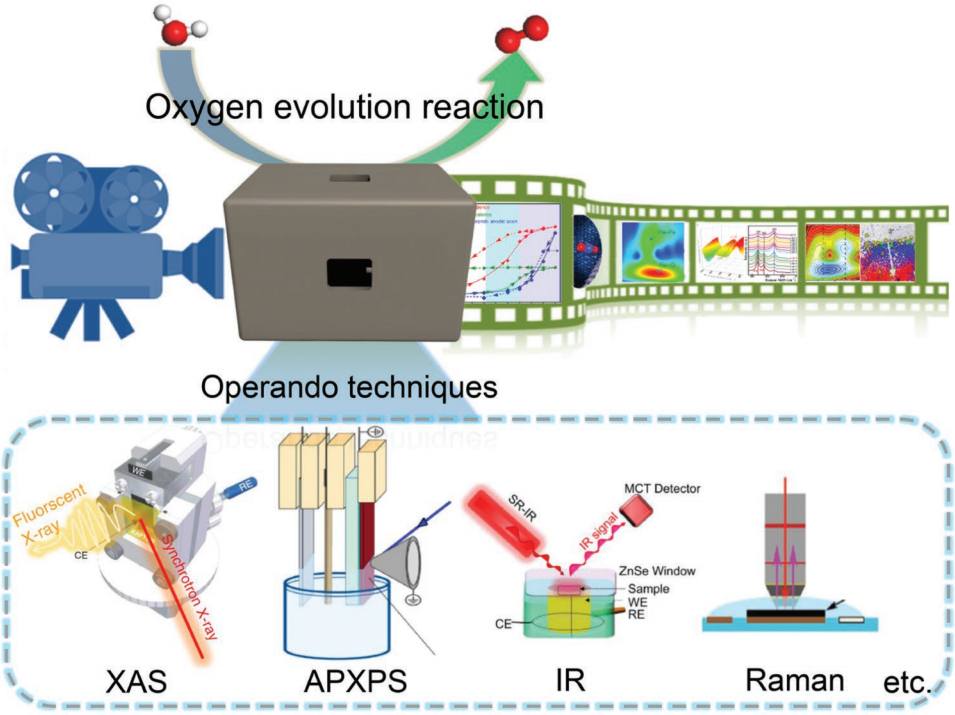

Figure 1. A schematic illustration of the operando characterizations for the OER.

For example, to track the morphological evolution of the catalyst during the OER potential cycling, identical location TEM has been performed by Shen et al. on the $Ba_{0.5}Sr_{0.5}Co_{0.8}Fe_{0.2}O_{3-\delta}$ (BSCF) perovskite OER catalyst, demonstrating a well preserved overall shape of the BSCF particle.[40] Further close-up identical location high-angle annular dark-field scanning transmission electron microscopy (HAADF-STEM) images captured during the OER potential cycling exhibit a rougher and more porous surface along with the OER potential cycling operation (**Figure 2**a). However, it is also possible that the structural evolution might come from the electron beam induced irradiation effect during the in situ experiment. As for another emerging in situ microscopy technique, that is, the in situ liquid cell TEM, the development of which requires thin but strong windows and is still in its infant stage.[41] This powerful technique can provide us the opportunity to closely observe the surface reconstruction and atom rearrangement at the solid-liquid interface, but is currently challenged by the technical design of the TEM holder, the inevitable electron beam damage to the sample, and the significantly reduced resolution in the in situ liquid cell.

In view of the above mentioned challenges and limitations of the in situ microscopy techniques to handle complex cases on the electrochemical three-phase solid-liquid-gas reactions, most of the reported microscopy characterizations of OER catalysts are based on ex situ or quasi-in situ measurements, collecting structure information of catalysts at the pristine and different stages.[14] For example, the morphology and phase structure changes of the crystalline $SrIrO_3$ OER electrocatalyst, which are shown to undergo an interfacial transformation from crystalline to amorphous structures at the surface region of the catalysts during the OER potential cycling in the acidic electrolyte, have been reported by Suntivich and co-workers using quasi-in situ cross-sectional TEM.[42] The overall thickness of the material does not change significantly while an amorphous layer quickly forms on the reaction interface after 0.25 h OER conditioning but almost stops evolving in the next few hours (Figure 2b). It is interesting to note that although the thickness of the amorphous layer does not evolve obviously from 0.25 to 4 h, however, the electrocatalytic OER performance keeps improving greatly. This indicates that the amorphous oxide layer further experiences an additional reconstruction process after the initial phase transformation, which might be related to an increasing disordered degree of the structure. This in situ activation process transforms the pristine crystalline $SrIrO_3$ into a highly disordered Ir octahedral network, and the reaction mechanism of the disordering-activity correlation calls for further theoretical investigations.

Traditional noble metal-based OER electrocatalysts using bulk nanoparticle or thin film materials exhibit outstanding OER activity in acidic water electrolyzes but are facing great challenges in large-scale commercialization due to their high expense. Based on the current situation, isolated Ir sites anchored in a non-noble metal Co_3O_4 host has been recently probed by Qiao and co-workers via the quasi-in situ high resolution (HR)STEM technique, demonstrating an effective strategy to reduce the noble metal content in the OER electrocatalyst while achieving excellent anti-acidic corrosion stability and outstanding OER activity.[36] HAADF-HRSTEM investigation for the fresh Ir-doped Co_3O_4 catalyst manifests that the isolated Ir centers are accommodated into the cationic sites of the Co_3O_4 host without the formation of Ir oxide nanoparticles (Figure 2c). Moreover, the statistical analysis on thousands of

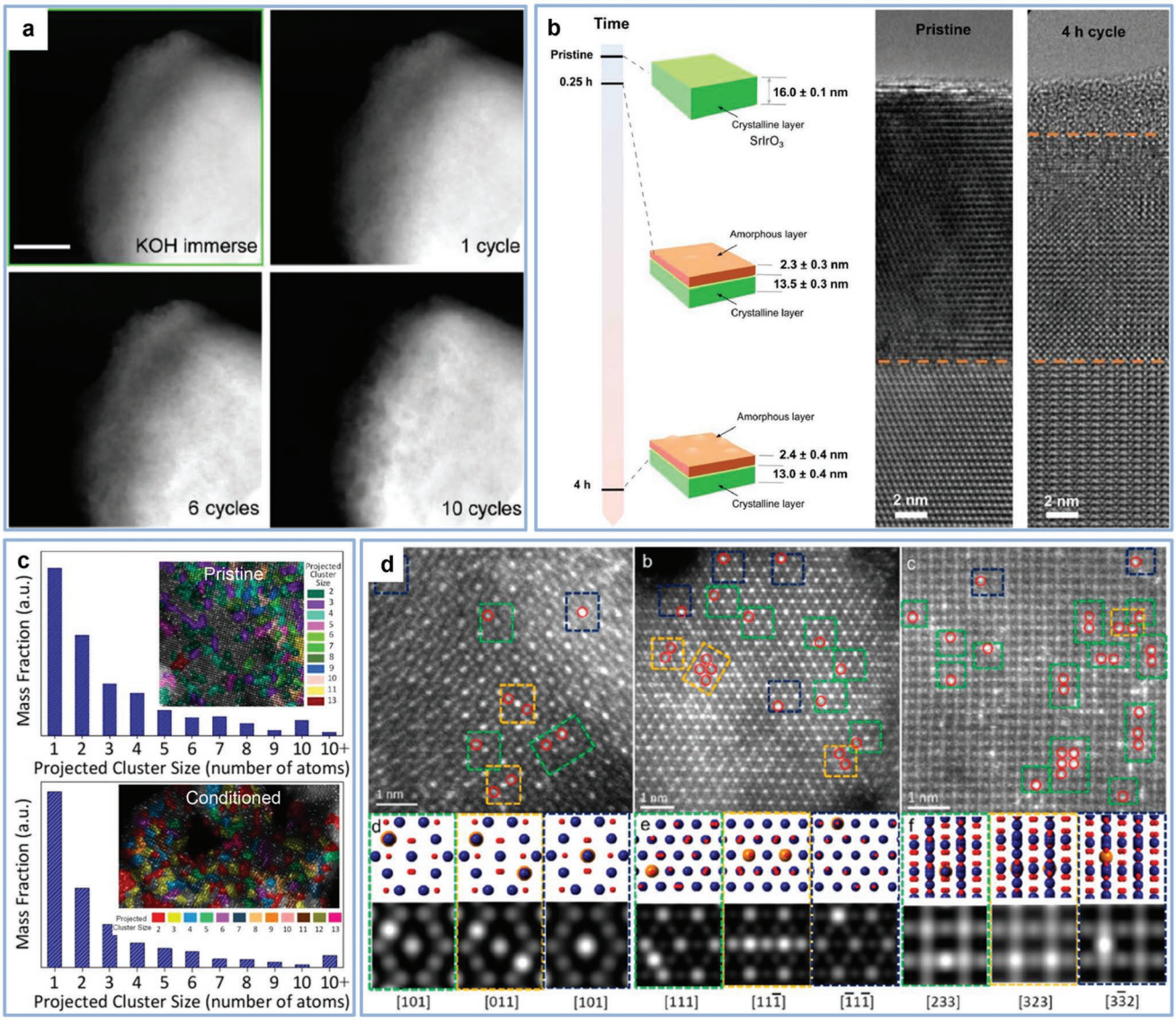

Figure 2. a) HAADF-STEM images of BSCF catalyst along with potential cycles. Reproduced with permission.[40] Copyright 2020, American Chemical Society. b) A schematic illustration of the surface amorphization process of the $SrIrO_3$ crystalline layer and the cross-section TEM images of the materials at the pristine stage and after 4 h OER operation. Reproduced with permission.[42] Copyright 2021, American Association for the Advancement of Science. c) HAADF-HRSTEM images, cluster distribution graphs, and mass fraction histograms with different numbers of Ir clusters for pristine and OER-conditioned Ir-doped Co_3O_4 catalyst. d) HAADF-HRSTEM images and the corresponding structural projections along varying symmetry-related directions of the OER-conditioned Ir-doped Co_3O_4 catalyst. Reproduced with permission.[36] Copyright 2021, American Chemical Society.

Ir atoms demonstrates the isolated Ir atoms in the catalyst are highly dispersed. To study the structural evolution of the catalyst after the OER operation, quasi-in situ HAADF-HRSTEM characterization and statistical analysis were also performed on the OER-conditioned catalyst, which demonstrates well-preserved short-range correlation of Ir sites. Atomic-resolution STEM image based on [011], [111], and [233] projections of the OER conditioned catalyst in the acidic electrolyte demonstrates well-dispersed individual Ir centers with a brighter contrast (Figure 2d). The strong interaction between Ir atoms and Co_3O_4 host enables the Ir-doped Co_3O_4 catalyst to exhibit outstanding corrosion resistance in harsh acidic solutions and applied electrochemical oxidative potentials, which is responsible for the significantly improved OER activity and stability in acidic electrolyte compared with the parent Co_3O_4 catalyst.

4. XAS

XAS is inner-shell spectroscopy that collects information of interactions between the incoming X-rays and the core electrons within atoms. The XAS spectra can be divided into two regions. The first part is the X-ray absorption near edge structure (XANES), which reflects element-specific information of the electronic structure, the bonding geometry of the absorbing atom, and the density of unoccupied states. The second region

is the extended X-ray absorption fine structure (EXAFS), which provides information on local structures involving bond distances and coordination numbers around the absorbing atoms.[43] The XAS technique can reflect the ensemble structure information of the whole catalyst and is proven to be a powerful approach to study the electrochemical OER by designing thin-film or thin-walled electrocatalysts (<10 nm), considering the fact that the structural evolution of electrocatalysts mainly happens on the surface/subsurface region. This powerful technique has gained tremendously increasing research efforts in probing the element-specific information on the electronic and geometric structures of materials in recent decades.[30,44–49] Thanks to the development of operando XAS measurements, which has been extensively utilized to investigate the dynamic structural evolution of the catalysts in terms of both coordination environments and oxidation states of active centers under real working conditions, excellent correlations between the structure and the electrocatalytic performance have been established.[30] Such useful information provides us precious opportunities to understand the role of catalytic materials during catalysis, identify the active centers and unravel the reaction mechanism. To get a more intuitive impression, a cartoon illustration showing a representative custom-designed operando XAS cell has been depicted in **Figure 3**a. In this section, we will highlight some recent advances in terms of applying operando XAS technique in monitoring the structural evolution of OER electrocatalysts with a focal point on the local coordination environment using EXAFS analysis and the oxidation state via XANES and soft XAS strategies.

4.1. Coordination Environment Evolution

Basically, the coordination environment of the reactive centers involves two important parameters, that is, the bond length and the coordination number, which can be provided by the time-resolved EXAFS analysis extracted from the operando XAS experiments. In EXAFS analyses, the key characteristics of the local structure of the materials can be captured by the radial distribution function, which contains rich information in terms of the number of nearest neighboring atoms, interatomic distances, and degree of structure disorder, all crucial to the reaction mechanism understandings.[30] Therefore, such important structure information is used to establish important correlations between the structure of catalytic centers and the activity of catalysts using quasi-operando and operando XAS experiments. Here we start from the quasi-operando XAS characterizations to determine the coordination environment of catalytic reactive centers, which have been widely used to study the structural transformation phenomenon during the OER process. For example, Wu et al. have recently probed the structural evolution of the Ni—Fe selenide as the pre-catalyst of the OER (Figure 3b).[10] The EXAFS fitting results show the disappearance of the Ni—Se bond and the emerging Ni—M and Ni—O bonds in the catalyst after the OER operation, which substantiates the successful conversion from the initial selenide to the post-formed oxyhydroxide structure. Interestingly, the post-formed Ni—Fe oxyhydroxide catalyst exhibits much higher OER activity than that of the Ni—Fe oxide counterpart. As demonstrated by the quasi-operando EXAFS analyses, the boosted OER performance is found to be originated from the manipulated local coordination structure distortion and disordering which are inherited from the selenide pre-catalyst. However, quasi-operando experiments fail to reflect the structure changes caused by the applied electrochemical potential, which is very crucial to study the reaction mechanism under the real working conditions and can be achieved by operando XAS experiments.

On that account, we then show some recent examples using operando XAS experiments to study the OER, starting from an important group of materials, that is, metal-organic frameworks (MOFs) and derivatives as OER electrocatalysts.[8,9,11,13,50–52] By applying the operando XAS technique, Zhao et al. have probed the structural transformation of a NiCo-MOF-74 material during the OER process.[13] A close examination of the coordination environment of metal active centers is determined by Fourier transform (FT)-EXAFS analysis under operando conditions (Figure 3c,d). The NiCo-MOF-74 catalyst experiences a two-step dynamic structural evolution. At the resting stage with an applied electrochemical potential of 1.1 V (versus RHE), the NiCo-MOF-74 catalyst operando transforms into a structure similar to the standard β-$Ni(OH)_2$ phase. Subsequently, the structure of catalyst further reconstructs to the γ-NiOOH analog under the potential of 1.5 V (versus RHE) at the catalytic stage, which acts as the catalytically active phase toward the OER. The detailed coordination environment involving the bond lengths and coordination numbers of metal centers is analyzed by EXAFS during the operando OER condition. As shown in Figure 3c, the nearest-neighbor Ni-M (M denotes Ni or Co) and Ni—O bond lengths are greatly shortened when the applied electrochemical potential is greater than 1.3 V (versus RHE), which agrees well with the bond length gap between hydroxide and oxyhydroxide analogs and further substantiates the structural evolution from metal hydroxide to metal oxyhydroxide. Moreover, the calculated coordination numbers of Ni-M and Ni-O shells in the catalysts at the catalytic stage demonstrate the operando generated oxygen vacancies in the catalytically active oxyhydroxide analog considering the saturated six-coordination configuration. The authors believed that the operando generated γ-NiOOH analog derived from the MOF pre-catalyst via denser packing of edge-sharing [MO_x] polyhedral with decreased interatomic distance and unsaturated coordination environment is responsible for the outstanding OER activity.

Using operando XAS studies, Zhang and co-authors have investigated the structural evolution process of the NiFe Prussian blue analog (PBA), which is an important group of MOF structures and is proven to be efficient OER electrocatalysts (Figure 3e).[53] The authors first conclude that the pristine PBA catalyst operando transforms into the $Ni(OH)_2$ structure as the active species for the OER. Thereafter they identify that the operando generated $Ni(OH)_2$ analog allows the deprotonation process under the applied potential to form NiOOH species which contains high-valence Ni^{4+} species acting as the OER active site. Operando EXAFS fitting results demonstrate the Ni—O bond length shrinkage under the increasing applied electrochemical potentials, which substantiates the local structure of the catalysts transforms from the pristine PBA to $Ni(OH)_2$, and ultimately evolves to NiOOH, serving as the active site for the

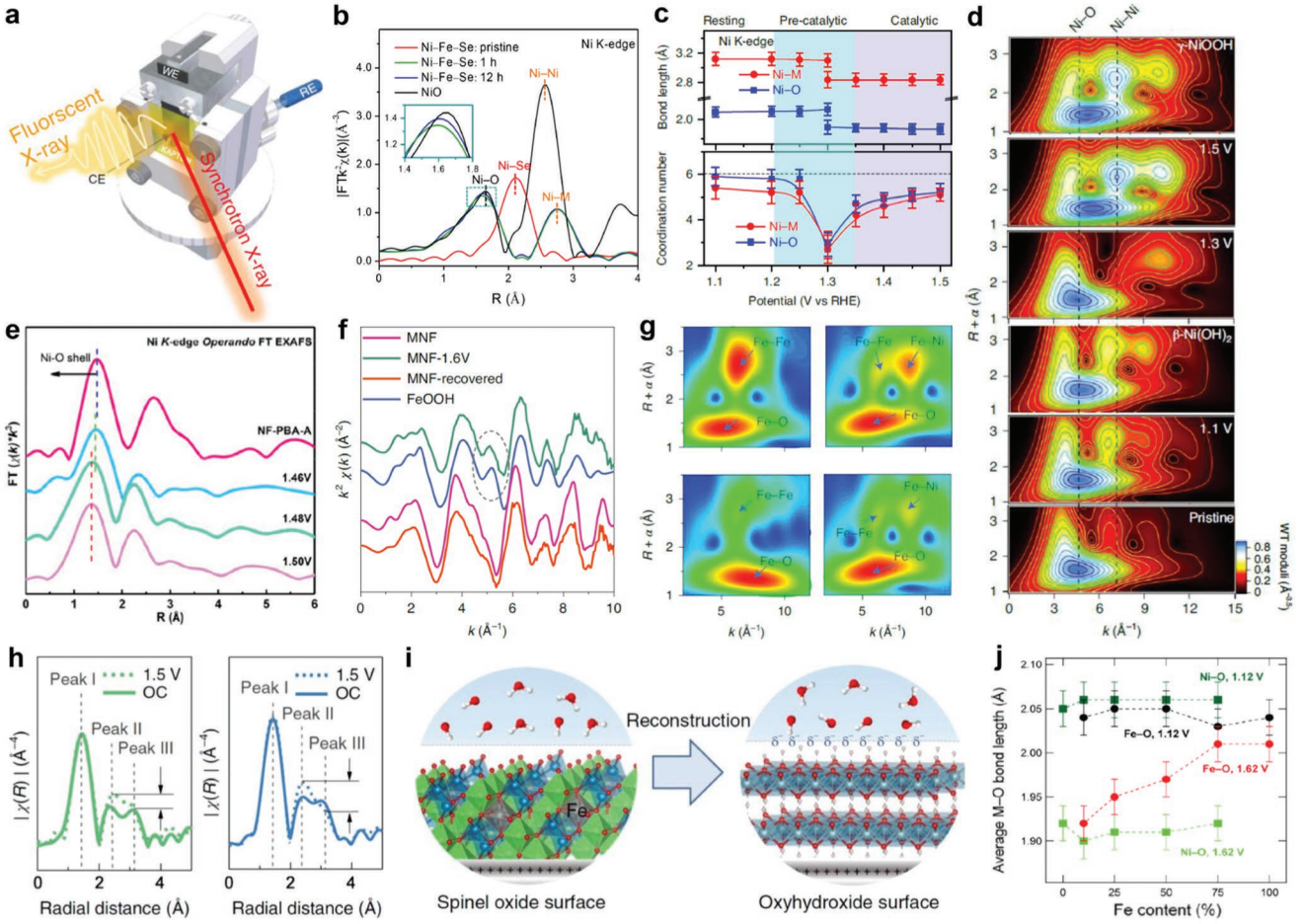

Figure 3. a) A schematic illustration of the custom-designed operando XAS cell. Reproduced with permission.[47] Copyright 2020, Nature Publishing Group. b) Ni K-edge EXAFS spectra of catalysts during the OER. Reproduced with permission.[10] Copyright 2021, Wiley-VCH. c) Evolutions of bond length and coordination number for the Ni-M and Ni-O coordination shells during the OER catalysis. d) Ni K-edge EXAFS wavelet transforms of NiCo-MOF-74 recorded at different potentials. Reproduced with permission.[13] Copyright 2020, Nature Publishing Group. e) EXAFS spectra of NF-PBA under different potentials. Reproduced with permission.[53] Copyright 2018, American Chemical Society. f) Fe K-edge EXAFS spectra and g) the corresponding wavelet transforms analysis for different samples. Reproduced with permission.[57] Copyright 2020, Nature Publishing Group. h) Co K-edge EXAFS spectra of $CoAl_2O_4$ (left) and $CoFe_{0.25}Al_{1.75}O_4$ (right) at the open circuit potential and 1.5 V (versus RHE). i) A schematic illustration of the reconstruction process of $CoFe_{0.25}Al_{1.75}O_4$ during the OER. Reproduced with permission.[14] Copyright 2019, Nature Publishing Group. j) Bond lengths extracted from the XAS spectra at different potentials as a function of the Fe content. Reproduced with permission.[58] Copyright 2015, American Chemical Society.

OER at the catalytic region. However, the coordination number of the first Ni-O shell almost remains constant throughout the whole OER potential cycling process, demonstrating the structural robustness of the octahedral Ni sites. In this example, by correlating with the electrocatalytic performance, the coordination environment evolution of active centers and the phase structural transformation obtained from operando XAS measurements during electrocatalysis provide valuable information in understanding of the OER reaction mechanism.

Besides MOFs structures and derivatives, operando XAS experiments have also been applied on 3d-transition metal-based (e.g., Ni, Fe, Co, etc.) hydroxides, oxides, and oxyhydroxides, which are well acknowledged as one group of the most promising OER electrocatalysts.[54–56] The reaction mechanism of the OER largely remains elusive due to the detection limitation of the current characterization approaches, the complex multi-phase interface reaction, and the dynamic structural evolution under operando conditions. The electrochemical activation process of oxides/hydroxides materials is a reflection of the structural evolution, which needs to be unraveled by operando experiments. Applying operando XAS approach on some model catalysts, the mystery in the black box is gradually unraveling. For instance, Kuai et al. have recently demonstrated the phase segregation reversibility in a NiFe hydroxide OER catalyst (Figure 3f,g).[57] EXAFS spectra and wavelet transformation (WT) analysis derived from operando XAS measurements reveal that the NiFe hydroxide is transformed into the FeOOH structure under the applied electrochemical potential at the OER operating region. After exposing the conditioned sample to the moist air for 2 days, the structure of catalyst largely recovers to the initial state while the catalytic activity toward the OER also recovers, demonstrating a novel strategy to enhance the catalyst stability. In this example, the FT analyses separate backscattering atoms by their radial distance from the absorbing atom, which provide

the structural information of the absorbing atom. However, the wavelet transform (WT) not only provides data at the radial distance resolution, but also resolves the data in k space, which eases the discrimination of atoms by their elemental nature, especially if these atoms are at the same distance.

The surface reconstruction of the Fe-substituted $CoAl_2O_4$ ($CoFe_xAl_{2-x}O_4$) spinel structure has been studied by Wu et al. via performing operando X-ray absorption fine structure (XAFS) measurements.[14] The electrochemical results manifest that the Fe substitution successfully facilitates the formation of Co oxyhydroxide, which is further substantiated by operando XAFS studies. The operando Co K-edge FT EXAFS spectra at regions of peak II and peak III demonstrate clear intensity increases after applying an electrochemical potential of 1.5 V (versus RHE), which strongly indicates the emergence and accumulation of Co atoms occupying the edge-sharing octahedral sites due to the formation of Co oxyhydroxide (Figure 3h). Moreover, Fe substitution in $CoAl_2O_4$ enables a much higher ratio of peak II to peak III in $CoFe_xAl_{2-x}O_4$ compared with that of $CoAl_2O_4$, which further reveals a more thorough surface transformation to oxyhydroxide in the presence of neighboring Fe species (Figure 3i). In another example, Friebel et al. have applied operando XAS experiments to study the active site in Ni-Fe-OOH OER electrocatalysts with varied metal ratios.[58] The determined Ni—O bond lengths can be assigned to α-$Ni(OH)_2$ and γ-NiOOH, respectively, at the resting and catalytic stages, regardless of the presence and concentration of Fe in the catalysts. Interestingly, at the OER catalytic stage, the average Fe—O bond length gradually stretches with the increasing Fe content toward that of the pure γ-FeOOH (Figure 3j). Such stretched bond distances are commonly associated with a decreased oxidation state. In consideration of the operando experimental results, further density functional theory (DFT) calculations reveal that the Fe sites serve as the OER active site rather than the Ni sites. However, there are still many aggressive debates on identifying the active site of bimetallic/multimetallic OER electrocatalysts, calling for more in-depth and comprehensive studies.

4.2. Oxidation State Evolution

Besides the coordination environment of the reactive centers in the catalysts can be determined by the EXAFS analyses, the identification of the oxidation state of active species in OER electrocatalysts is also very important to understand the OER reaction mechanism, which is under long-time debate in the current literature.[7,13,59–61] The oxidation states of elements are very sensitive to the position of the absorption edge, which is defined as the onset of transitions to delocalized continuum states and can change by a few eVs when the valence state of atoms change by one electron, at the XANES region.[30] A linear dependence relationship between the edge energy position of XANES and the oxidation state of the element has been proposed and demonstrated as an effective method to determine the oxidation states of specific elements in the catalysts.[62] Therefore, the XANES technique, which can reflect abundant useful information about the atomic and electronic structure of the material, has been widely applied to determine the oxidation state of atoms. Recently, tremendous efforts have been afforded on using quasi-operando and operando XANES technique for application in OER electrocatalysts to capture the oxidation state evolution of the active species. For example, Wu et al. recently have combined quasi-operando XANES analyses and theoretical calculations to demonstrate the OER active Ni site in a bimetallic Ni—Fe system.[10] The results show that the electronic structure of the OER active Ni site has been modulated by the surrounding Fe species due to the catalytic synergy, leading to the formation of low-valence state Ni centers with moderate bindings to some key OER intermediates (**Figure 4**a,b). In contrast, the binding strength of the key OER intermediates on Fe sites is too strong to activate the reaction. It is worth noting that the oxidation state of the active species in OER electrocatalysts is closely related to the applied electrochemical potential on the electrocatalysts under real working conditions, calling for operando XAS characterizations.[13]

The oxidation state evolution of the active centers, which is electrochemical potential-dependent and is critical to understand the intrinsic catalytic mechanism of the electrocatalytic oxygen evolution and can be well monitored by operando XANES and soft XAS techniques, often happens simultaneously with its coordination environment changes. By applying operando XANES studies, Su et al. have investigated the electronic structural evolution of a NiFe-PBA OER pre-catalyst as a function of the applied potential.[53] The increasing applied potential induces a gradually positive shift of the energy position of the absorption edge, indicating that the oxidation state of Ni species shifts to a higher valence state and the operando generated $Ni(OH)_2$ acts as the actual OER catalytic phase (Figure 4c). The great oxidation state change in the operando generated amorphous $Ni(OH)_2$ is in sharp contrast with a much smaller valance state change in the crystalline $Ni(OH)_2$. Importantly, control experiments confirm this potential-dependent process is reversible. This example substantiates the important role of operando XANES as a powerful tool to study OER electrocatalysts.

In another example involving a bimetallic NiCo-MOF structure as the OER electrocatalyst, Tang and co-workers have applied operando XANES to probe the correlation between the valence states of metallic centers and the electrocatalytic performance of the catalyst.[13] The Ni K-edge XANES spectra gradually shift to higher energy, indicating that the oxidation state of Ni species increases with the arising potential. Changes of the valence states of both Ni and Co species as well as the synchronous electrocatalytic performance as a function of the applied potential are analyzed, demonstrating a higher and reversible valence state variation loop of Ni upon the potential cycling compared with that of Co (Figure 4d). Moreover, a high oxidation state of 3.8 is observed on Ni species at an applied potential of 1.5 V (versus RHE) on the NiCo-MOF catalyst. Interestingly, such high Ni valence has not been captured on the Ni-MOF counterpart (Figure 4e). The results demonstrate the crucial role of Co by successfully regulating the oxidation state of the adjacent Ni species toward the OER active phase. The catalytic synergy introduced by Co facilitates the structural transformation to high-valence Ni oxyhydroxide in the bimetallic NiCo-MOF structure, and together with the optimized local coordination structure, therefore leading to the boosted OER activity.

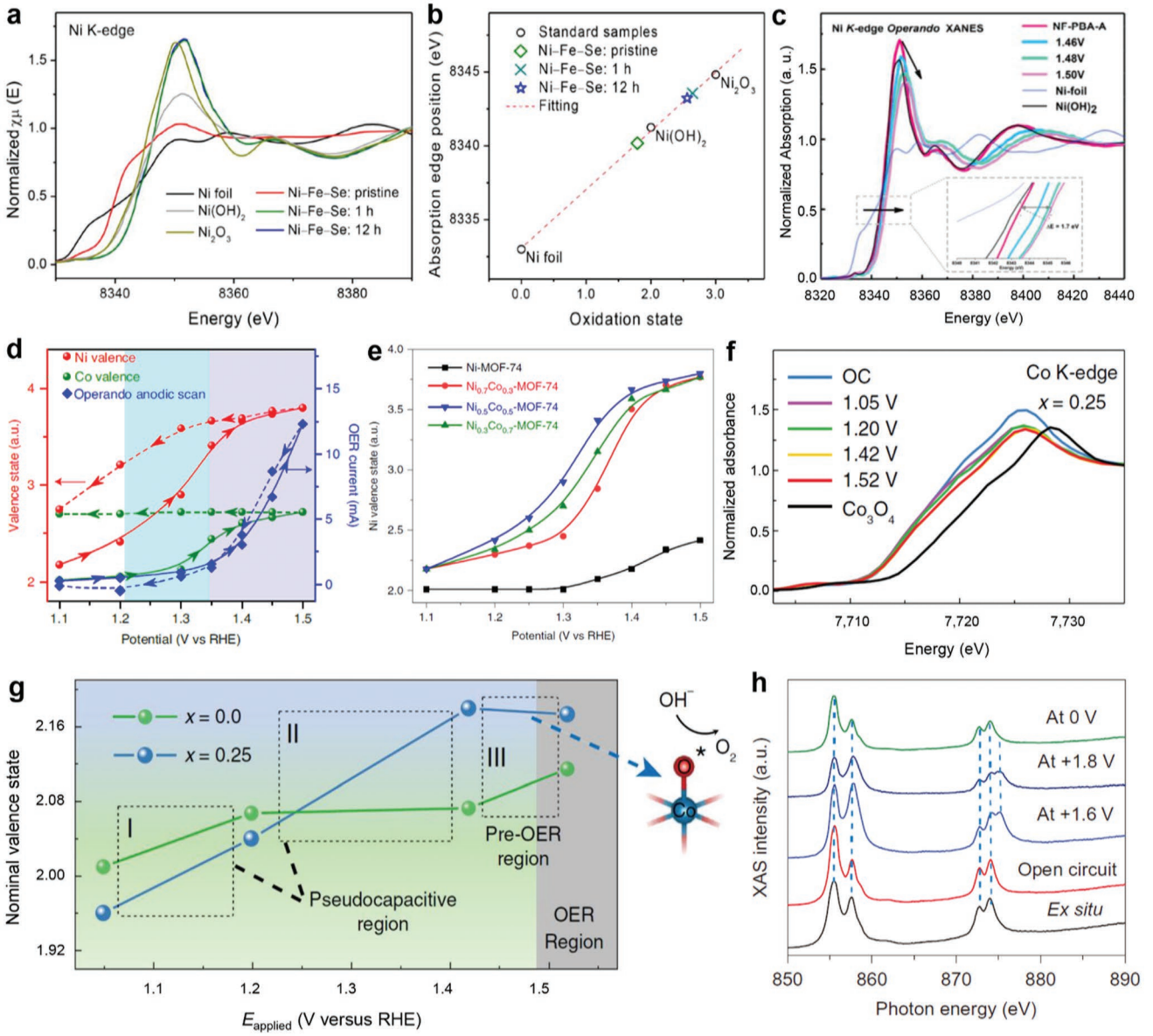

Figure 4. a) Normalized Ni K-edge XANES spectra, b) and correlation between the absorption edge position in XANES spectra and the oxidation state of Ni species in Ni—Fe—Se catalyst during the OER as well as reference samples. Reproduced with permission.[10] Copyright 2021, Wiley-VCH. c) Operando Ni K-edge XANES of NiFe-PBA at different applied potentials and reference samples. Reproduced with permission.[53] Copyright 2018, American Chemical Society. d) Changes of the Ni and Co valence states and the electrochemical OER current versus applied potential in NiCo-MOF. e) Change of the Ni valence states versus applied potential in different catalysts. Reproduced with permission.[13] Copyright 2020, Nature Publishing Group. f) Operando Co K-edge XANES analysis of $CoFe_{0.25}Al_{1.75}O_4$ under different potentials. g) Operando Co valence state evolution of $CoFe_{0.25}Al_{1.75}O_4$ and $CoAl_2O_4$ catalysts under different potentials. Reproduced with permission.[14] Copyright 2019, Nature Publishing Group. h) Ni L-edge of NiCoFeP catalyst at different working conditions. Reproduced with permission.[68] Copyright 2018, Nature Publishing Group.

To understand the enhanced OER activity in the $CoAl_2O_4$ spinel OER catalyst by Fe substitution and the dynamic oxidation state evolution of Co species, operando XANES analyses have been performed by Xu and co-workers.[14] The Co K-edge XANES of $CoFe_{0.25}Al_{1.75}O_4$ and $CoAl_2O_4$ spinel oxides under different electrochemical potentials are recorded under operando conditions (Figure 4f), both demonstrating Co K-edges shift to higher energy and hence indicating the oxidation of Co species. The dynamic Co valence state evolution as a function of the applied potential has been analyzed (Figure 4g). Co(II) in $CoFe_xAl_{2-x}O_4$ tends to be oxidized to Co(III) or an even higher oxidation state under the applied electrochemical potential during the potential cycling which is observed in the first cyclic voltammetry cycle, demonstrating an irreversible surface reconstruction from spinel oxide to oxyhydroxide. The oxidation state increase of Co can be regarded as a reflection of the deprotonation process on the reconstructed catalyst surface. The authors believe that Fe substitution in $CoAl_2O_4$ is responsible for facilitating the deprotonation process at the low potential region to form OER active phase by surface reconstruction,

and then leads to a much higher oxidation state of Co at the pre-OER region, which accounts for the boosted OER activity. This example further elaborates the catalytic synergy in bimetallic OER catalysts, demonstrating that high-valence state reactive centers have been observed with the assistance of neighboring auxiliary metal elements under OER working potential regions. In recent years, to investigate the complex OER process involving multi-active species, single atom catalysts (SACs) with well dispersed and clear structures are emerging as model catalysts. For example, some recent works on SACs have combined the operando XAS technique and DFT calculations and claimed that the active site of OER was either IrO_x or non-noble metal-based dual metallic site.[63–66] By applying operando XAS experiments, evidences were given on the valence state and coordination environment changes of elements in the catalysts during the reaction. However, poor connections were often presented in terms of the structure-activity correlations. The comprehensive understandings of the role of each element in the catalysts, the multi-electron transfer process, and the dynamic structural evolution process during the reaction, as well as the identification of the real active sites and the reaction mechanisms, are calling for close combinations of operando XAS with other operando techniques as well as theoretical calculations.

The deep penetration of hard X-rays in XAS measurements provides a sufficient flexibility in terms of the sample conditions and environments, thus fully realizing the operando studies in electrocatalysis.[30] Beyond that, spectroscopic studies using the soft XAS technique (with X-ray energy range below 5 keV), as a surface sensitive technique due to its limited probe depth, can reflect more detailed electronic structure information at the surface region of the electrocatalysts. Moreover, L-edges (or even M-edges) of transition metals accessed by soft XAS are more sensitive to the oxidation state of the sample than K-edges.[67] For example, Sargent and co-workers have employed an operando electrochemical flow cell for operando soft XAS characterizations on a NiCoFeP OER electrocatalyst.[68] The operando soft XAS results demonstrate a Ni oxidation state evolution from Ni^{2+} to Ni^{3+} and Ni^{4+} upon the applied electrochemical potential on the catalyst, and more importantly a successful direct view confirmation of the operando generated Ni^{4+} species during the water oxidation (Figure 4h). Control experiments indicate that the incorporation of Fe, Co, and P beneficially optimizes the electronic structure of Ni oxides and hence facilitates the formation of Ni^{4+} species which is favorable for the OER. In another study on a FeCoW OER catalyst, Zhang et al. have performed ex situ soft XAS experiments in the total electron yield (TEY) mode to probe the oxidation state evolution of metal elements during the OER.[69] The results show that the surface Fe^{2+} has been fully oxidized to Fe^{3+} at an applied potential of 1.4 V (versus RHE) on both gelled and annealed FeCoW catalysts. However, the valence states of Co in two samples are quite different at 1.4 V (versus RHE), and both reveal a remarkable percent of Co^{2+} species on the catalyst surface, which are found to be much less reactive by DFT calculations. An important advantage of soft X-ray technique is its high resolution in energy (<0.1 eV) because of the long life of the core states, which results in the spectra sensitive to details of the electronic structure properties, such as the valence, spin state, and the symmetry. However, soft XAS technique is still facing critical challenges in terms of the low-energy X-ray attenuation by air and its limited probe depth, which hence complicates the design of the operando cell and constrains the measurements in operando electrochemical reactions, because the operando cell is required to be integrated into the beamline setup while separating the samples from vacuum via X-ray transparent thin windows.[30]

5. Other X-Ray-Related Techniques

Besides the powerful operando XAS techniques in determining the coordination environment and the oxidation state of key elements in OER catalysts during the reaction operation, other commonly used in situ/operando X-ray-related techniques typically involving XPS and XRD are able to provide the electronic and crystal structure information, respectively, which are helpful to combine with other characterization approaches to unravel the complex OER reaction mechanism.

5.1. XPS

XPS is a surface-sensitive quantitative technique, which can provide fingerprint element-specific chemical and electronic state structure information of samples. However, the application of in situ XPS in electrocatalysis is challenged by the requirement of the ultra-high vacuum condition at the electrode-electrolyte interface.[70] Nevertheless, quasi-in situ XPS studies are able to probe some preliminary surface structural evolution information before and after the electrochemical tests.[10] For example, Mayrhofer and co-workers have successfully probed the surface reconstruction process of Ir-based electrocatalyst after OER operations for certain periods of time using quasi-in situ XPS technique.[71] The average electronic structure information detected by quasi-in situ XPS in regions of Ir 4f and O 1s and valence-band spectra demonstrates a gradual surface structural transformation from metallic Ir to IrO_2 during the first 120 h operation (**Figure 5**a). Challenges of the quasi-in situ XPS involve the inevitable exposure of samples to air and the disconnection to the applied electrochemical potential, where the oxidation state of the catalyst surface would be changed. Therefore, it fails to capture the real catalyst surface structure which is in close correlation with the catalytic performance. This has greatly stimulated the recent development of the cutting-edge in situ ambient pressure XPS (APXPS), which requires a thin liquid layer of less than 20 nm (Figure 5b).[72]

In a recent study, Favaro et al. have applied in situ APXPS technique on a quinary $(Ni\text{-}Fe\text{-}Co\text{-}Ce)O_x$ OER electrocatalyst and observed the catalyst surface chemical structural evolution clearly under the applied electrochemical potential (Figure 5c).[73] The XPS spectrum at Ni 2p region for the pristine catalyst exhibits a typical rock-salt NiO structure with Ni (II) species. Under the open circuit potential (OCP), the $Ni^{(II)}O$ structure undergoes a partial conversion to $Ni^{(II)}(OH)_2$. The further partial oxidative conversion from Ni (II) to Ni(III) as a reflection of the formation of $Ni^{(III)}OOH$ phase, which is commonly believed as the OER active phase, under the OER catalytic stage has also been observed by APXPS. Similarly, Co shows a

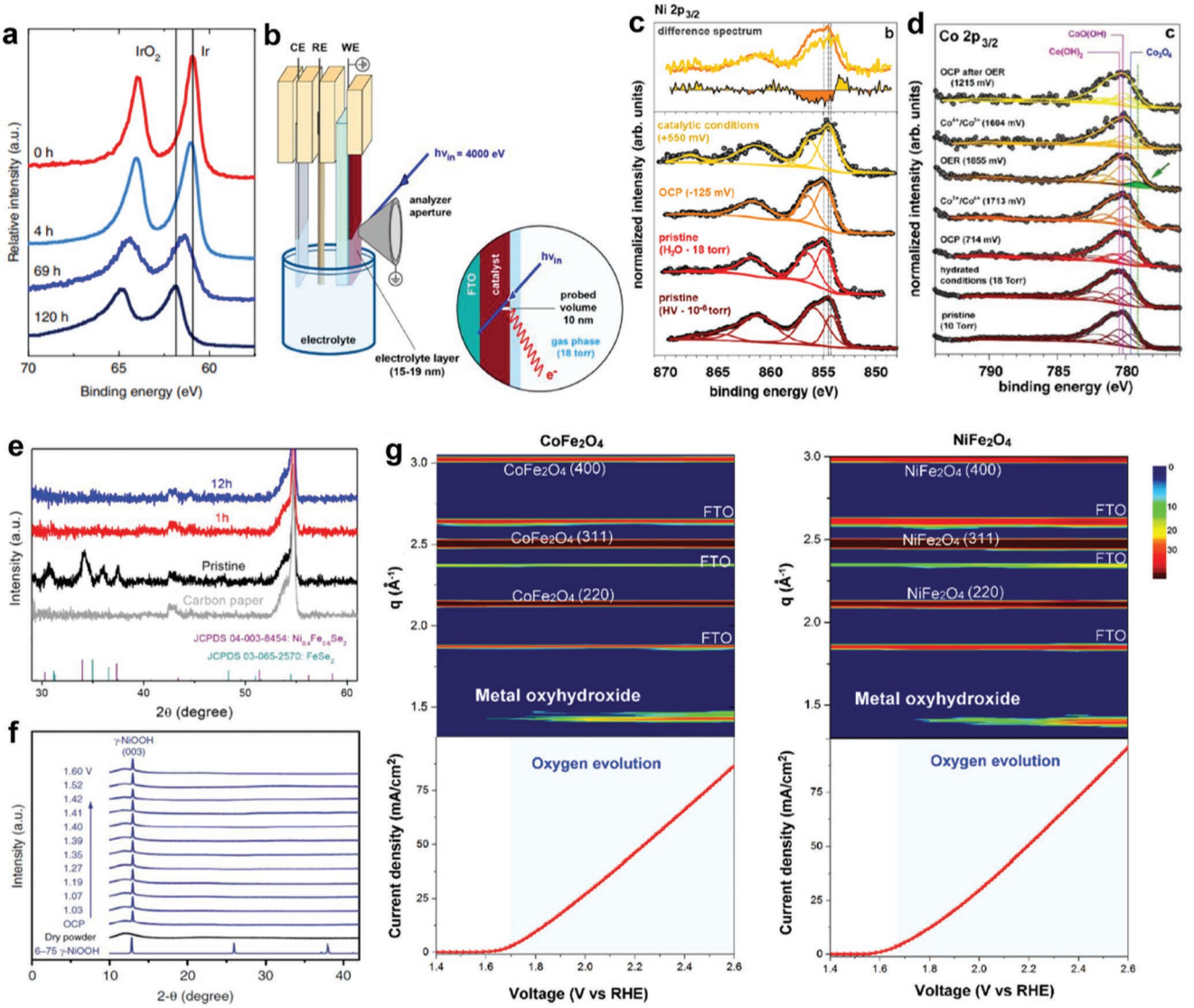

Figure 5. a) XPS spectra in the region of Ir 4f of the Ir-based electrocatalyst during the OER operation. Reproduced with permission.[71] Copyright 2018, Nature Publishing Group. b) Schematic illustration of the APXPS setup. c) Operando APXPS in the region of Ni $2p_{3/2}$ of $(Ni\text{-}Fe\text{-}Co\text{-}Ce)O_x$ catalyst at different conditions. Reproduced with permission.[73] Copyright 2017, American Chemical Society. d) Operando APXPS in the region of Co $2p_{3/2}$ of the biphasic CoO_x catalyst under different conditions. Reproduced with permission.[74] Copyright 2017, American Chemical Society. e) Quasi-operando XRD patterns of the Ni-Fe diselenide OER catalyst during the OER operation. Reproduced with permission.[10] Copyright 2021, Wiley-VCH. f) Operando XRD patterns of the $NiCeO_xH_y$ catalyst under different potentials. Reproduced with permission.[76] Copyright 2018, Nature Publishing Group. g) Operando grazing-angle XRD singles of $CoFe_2O_4$ and $NiFe_2O_4$ catalysts at different voltages. Reproduced with permission.[77] Copyright 2017, The Royal Society of Chemistry.

progressive change from the structure of the mixed oxides in the pristine catalyst to a $Co^{(II)}(OH)_2$ dominated structure under the OCP. When further applied at the OER catalytic region, the Co $2p_{3/2}$ experiences a downward binding energy shift, which reflects the further partial oxidation from $Co^{(II)}(OH)_2$ to $Co^{(II,III)}O_x(OH)_y$ species. The above in situ APXPS results confirm the structural evolution from Ni/Co oxide or $Ni/Co(OH)_2$ to an OER active phase of Ni/Co oxyhydroxides at the OER operating conditions. The authors further take the advantage of the in situ APXPS technique to unravel the nature of chemical structural transformation from the initial $Co(OH)_2$ or Co_3O_4 phases to Co oxyhydroxide under the applied anodic potential (Figure 5d).[74] Interestingly, the biphasic $Co(OH)_2/Co_3O_4$ material undergoes a partial surface phase transformation from $Co(OH)_2$ to CoO(OH) at the OCP and further experiences a complete structure oxidative evolution to CoO(OH) at the $Co^{3+} \rightarrow Co^{4+}$ transition region, which is prior to the OER catalytic region. The in situ generated CoO(OH) phase accounts for the high OER activity of the catalyst. This study demonstrates the presence of top surface $Co(OH)_2$ on the Co_3O_4 facilitates the structural transformation to the OER active phase CoO(OH), which is also tested to be stable in the OER durability test. It is noted that a close combination of in situ XPS and operando XAS techniques is encouraged to obtain more comprehensive

structural evolution information involving both electronic structure and coordination shell environment changes of the active sites during the OER catalysis.

5.2. XRD

Another important operando technique involves operando XRD, which can track the structural evolution of catalyst in terms of the phase structure type, the degree of crystallinity, and the crystallite particle size.[75] Compared with other characterization methods such as XAFS analyses by detecting the valence state and the coordination atmosphere of active species, the crystal structure of OER electrocatalysts as determined by XRD is relatively less potential dependence. The structural evolution process of the NiFe-based selenide as the OER pre-catalyst has been recently probed by Wu et al. using the quasi-operando XRD approach, demonstrating a clear crystal structure change after the OER operation, which is a reflection of the structural transformation from selenide to oxyhydroxide structure (Figure 5e).[10] Operando XRD is challenging in probing OER electrocatalysts but is very useful. For instance, Yan et al. have performed operando XRD analyses on $Ni(OH)_2$ and $NiCeO_xH_y$ materials both supported on the nickel foam to exclude the masking effect from the graphitic substrate.[76] After a short soaking in the alkaline electrolyte, both pristine $Ni(OH)_2$ and $NiCeO_xH_y$ catalysts exhibit remarkably increased crystallinities (Figure 5f). At the operando condition under the applied potential at the catalytic region, the $Ni(OH)_2$ catalyst transforms to a mixed-phase structure of β-$Ni(OH)_2$ and γ-NiOOH, which is dominated by the latter. In contrast, the $NiCeO_xH_y$ catalyst only shows a single γ-NiOOH phase under the applied potential. The authors believe that the incorporation of Ce in Ni hydroxide modulates the electronic structure of Ni species and facilitates the structural evolution to γ-NiOOH, which are both responsible for the boosted OER kinetics.

In another example, operando grazing-incidence XRD has been performed on the spinel oxide OER catalysts in a recent work reported by Chen and co-workers.[77] 2D contour maps of Bragg reflections and the OER current density as a function of the applied potential demonstrate the structural evolution of $CoFe_2O_4$ and $NiFe_2O_4$ spinel oxides during the OER (Figure 5g). At the OER catalytic region (>1.6 V versus RHE), a new peak emerges at a q value of ≈1.4 $Å^{-1}$, representing the formation of metal oxyhydroxide. Further analyses demonstrate this emerging peak can be assigned as β-MOOH phase acting as the OER active phase instead of the γ-MOOH analog. Compared with tremendous works reported on operando XAS characterizations, the traditional operando XRD might not be a suitable and powerful tool to collect informative signals on OER electrocatalysts, especially for samples with amorphous structure or low crystallinity at the surface or near surface regions close to the electrode-electrolyte interface. This puzzle can be solved by applying high-energy XRD (HE-XRD, >100 keV) with deep penetrations to the materials, which would enable the successful capture of the structure information of materials regardless of the amorphous or crystalline nature. Assisted by pair distribution function (PDF) analyses and reverse Monte Carlo simulations, operando HE-XRD technique can capture the structural evolution process of catalysts at the atomic level by analyzing the interatomic fine structures of catalysts at the second-level time resolution.[78,79] In addition, the structural transformation of OER catalysts often happens at the surface/subsurface regions with limited thickness, which cannot be selectively reflected by XRD, HE-XRD, and even for XAS as bulk information sensitive approaches. Design and fabricating materials with 2D ultrathin layers/films or in hollow structure with ultrathin walls are more suitable for operando XRD, HE-XRD, and XAS characterizations. In this way, most active centers in the catalysts can be exposed to the electrode-electrolyte interface to participate in the catalytic reaction.

The above mentioned in situ/operando X-ray-related techniques are demonstrated to be powerful tools to study the coordination and electronic structures of OER electrocatalysts under working conditions. However, extra attention should be paid to some X-ray sensitive materials, such as MOFs as OER electrocatalysts. This is especially important when using high-intensity light sources, such as laser light and synchrotron radiation, which can cause damage to the target samples. Control experiments should be carefully performed to rule out the influence from the X-ray damage on the catalysts, aiming at obtaining more solid structure information of catalyst induced by the catalytic process. Moreover, using quick scanning techniques can reduce the doses received by the samples, which hence alleviates the X-ray damage.

6. Other Characterizations

The structural evolution of catalysts during the OER operation can be monitored using a variety of other operando characterization methods.[15,80] For example, optical Raman and IR spectroscopy are fingerprint tools to identify the vibration modes of key intermediates during the reaction; on-line ICP-MS technique can analyze the metal dissolution results which are associated with the durability of catalysts; atom probe tomography (APT) can map out the 3D chemical species distribution changes during the structural evolution process of the OER; electrochemical impedance spectroscopy (EIS) can investigate the charge transfer resistance evolution of catalysts during the reaction; and so on. In this section, we will elaborate on these commonly used typical in situ/operando approaches with examples on studying OER electrocatalysts.

6.1. Raman Spectroscopy

Raman spectroscopy is a versatile characterization method widely used in studying the electrochemical reactions at the solid-liquid interface thanks to the weak Raman scattering of water compared with that of the IR spectroscopy.[81] Moreover, Raman spectroscopy can detect signals in the low-wavenumber region, which are often associated with metal-related bonds for identifying the catalytic active sites and the key intermediate species, but are inaccessible in the IR spectroscopy.[82] The weak Raman scattering signal can be enhanced by the surface enhanced Raman scattering (SERS), tip-enhanced Raman spectroscopy, and shell-isolated nanoparticle-enhanced

Raman spectroscopy (SHINERS), etc.[82–84] In recent decades, the rapid development of in situ Raman technique realizes its wide applications in the fields of catalysis.[85] In OER, in situ Raman spectroscopy has been widely used to determine the surface structural evolution which is highly potential-dependent (**Figure 6**a).[86] For example, Chen and co-workers have probed the gradual phase transformation from $NiCeO_xH_y$ to γ-NiOOH via performing the in situ Raman spectroscopy, as indicated by the emerging Raman peaks at 474 and 554 cm^{-1}.[76] The results show that the incorporation of Ce in the catalyst reduces the barrier and hence facilitates the phase transformation process at a low potential of 1.27 V (versus RHE), which is much lower than that of $Ni(OH)_2$ as the starting precursor (Figure 6b). Consequently, the $NiCeO_xH_y$ catalyst shows a much better OER activity than that of $Ni(OH)_2$. Similar conclusion has been drawn in a bimetallic NiFe spinel oxide OER catalyst, where the photothermal heating method facilitates the phase transformation process from oxide to γ-NiOOH at a lower potential than the catalyst prepared by the conventional approach (Figure 6c).[87] Interestingly, a lower potential for the phase transformation to OER active phase γ-NiOOH often can be linked to a superior OER activity. The emerging Raman characteristic peaks at 474 and 554 cm^{-1} can be assigned to the γ-NiOOH analog. However, in situ Raman studies often fail to identify the formation of FeOOH species due to the overlapping of the characteristic peaks of FeOOH with other Raman peaks and the relatively lower distribution of FeOOH species on the catalyst surface region.[87]

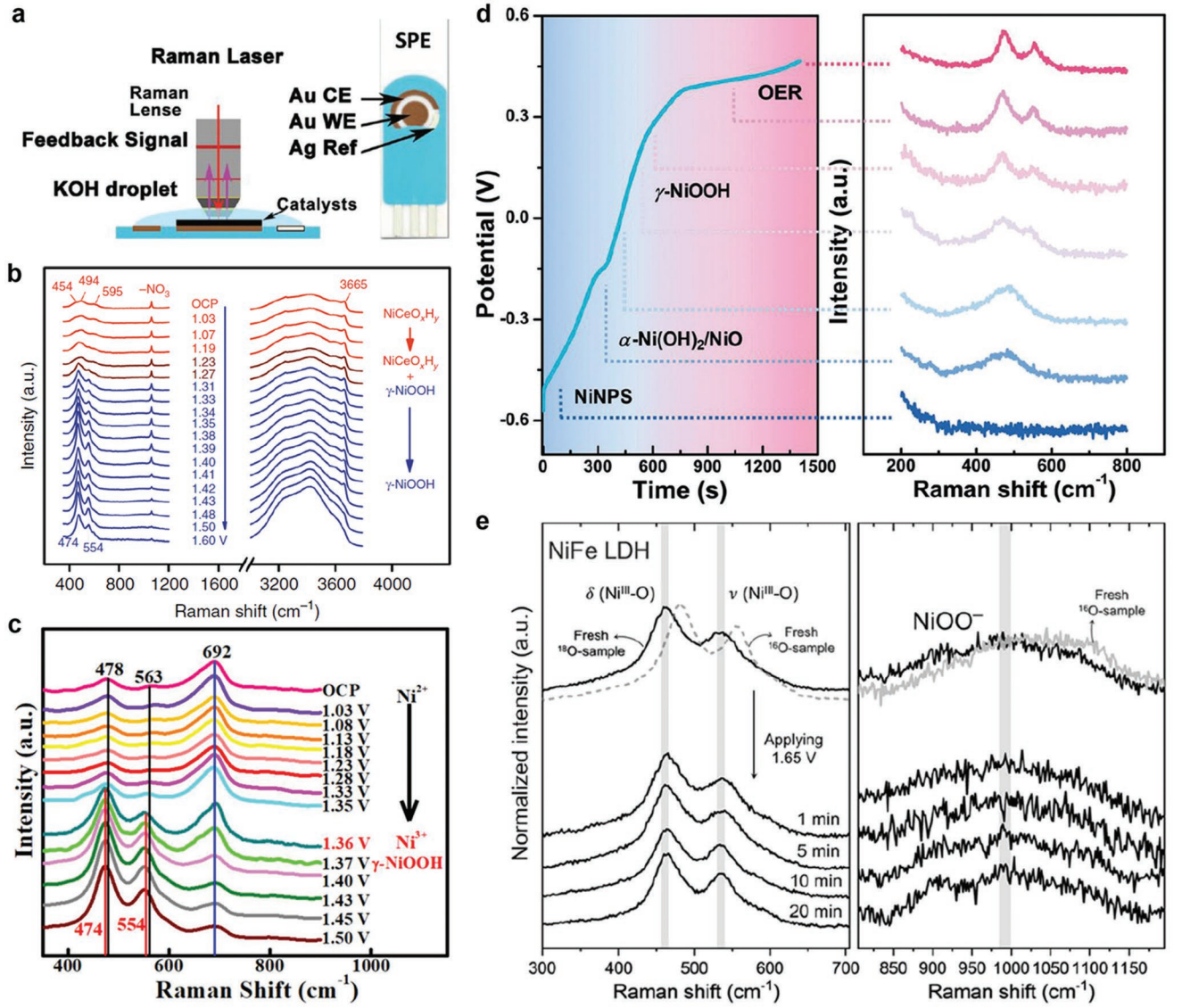

Figure 6. a) Schematic illustration of the operando Raman spectroscopy setup. Reproduced with permission.[86] Copyright 2020, The Royal Society of Chemistry. b) Operando Raman spectra collected at different potentials for $NiCeO_xH_y$ catalyst. Reproduced with permission.[76] Copyright 2018, Nature Publishing Group. c) Operando Raman spectra of NiFe oxide catalyst at varying applied potentials. d) Chronopotentiometry measurement and the corresponding operando Raman spectra for NiNPS catalyst. Reproduced with permission.[88] Copyright 2019, Wiley-VCH. e) Operando Raman spectra of ^{18}O-labeled NiFe LDHs. Reproduced with permission.[61] Copyright 2019, Wiley-VCH.

In a recent study using Ni-based pnictide/sulfide (NiNPS) as the OER pre-catalyst, Huang et al. have applied in situ Raman spectroscopy to track the structural evolution process during the OER.[88] The combination of the time-dependent potential plot at a low current and in situ Raman investigations successfully demonstrates a two-step structural evolution from the pristine NiNPS structure to the α-$Ni(OH)_2$/NiO phase and then to the γ-NiOOH species before the OER catalytic region (Figure 6d). The phase transformation from NiNPS to α-$Ni(OH)_2$ is irreversible, however, the structural evolution between $Ni(OH)_2$ and γ-NiOOH is reversible depending on the applied anodic potential on the catalyst. The OER reaction mechanism in terms of the active site in highly active NiFe (oxy)hydroxide is a long-time debate in the field.[59,60,89] On account of this, Lee et al. have combined ^{18}O-labeling experiments and in situ Raman spectroscopy to study the role of lattice oxygen in a set of Ni-based layered double hydroxides (LDHs).[61] The results demonstrate that the lattice oxygen participates in the reaction for Ni and NiCo LDHs, but is not involved in the catalysts of NiFe and NiCoFe LDHs (Figure 6e). The bulk Ni sites in the form of $NiOO^-$ in Ni and NiCo oxides are determined as the OER active phase. The incorporation of Fe in Ni-based LDHs changes the nature of the OER active site and also remarkably enhances the activity. These elaborated examples using traditional in situ Raman spectroscopy demonstrate it is a powerful tool to track the phase structural transformation of the catalysts, but it often fails to determine the corresponding reaction intermediates due to the corresponding weak Raman signals. We suggest and anticipate the further developments and applications of novel SERS techniques, for example, in situ electrochemical SHINERS,[90] coupled with other in situ/operando methods and DFT calculations to study the reaction mechanisms of the OER.

6.2. IR Spectroscopy

IR spectroscopy can provide fingerprint identifications of the polarized radical group for the key oxygen-related intermediates involved in the OER and concentrated within the window of 800–1600 cm^{-1}, which is highly vulnerable to water absorption.[33] A couple of strategies, for example, synchrotron radiation (SR) light source which provides a higher IR light intensity and surface-enhanced IR absorption (SEIRA) have been utilized to enhance the surface vibration signals.[33,91] Challenges involving short lifetime and limited quantities of the electrochemical reaction intermediates at the catalyst surface are urgently calling for in situ/operando IR techniques. Liu's research group has recently developed the operando SR-IR methodology in studying the OER reaction mechanism (**Figure 7**a). The absorption of IR signals in water has been effectively reduced using the capillary permeation of the porous working electrode with controlled thickness. Using operando SR-Fourier transform IR spectroscopy (SR-FTIR) technique, they studied the OER reaction mechanism of a metal-free amino-rich carbon material as an efficient OER electrocatalyst.[92] The results show that a new vibrational absorption band at 1546 cm^{-1} emerges, which can be assigned to the vibration stretching mode of *O—C species, when an electrochemical potential of 1.35 V (versus RHE) is applied (Figure 7b). Further operando control experiments reveal that this new IR peak is highly potential-dependent, demonstrating $H_2N—C{=}C$ group in the catalyst serves as the active site for the OER and its structural evolution to $H_2N—(*O—C){=}C$ by adsorbed *O intermediates during the OER (Figure 7c). Another fascinating example using operando SR-FTIR reported by Cheng et al. involves a lattice-strained NiFe-MOF as the OER electrocatalyst.[11] At the OER catalytic region when an electrochemical potential of 1.6 V (versus RHE) is applied on the catalyst, a new absorption band at 1048 cm^{-1} in the SR-FTIR spectra is observed, which can be assigned to the surface intermediates of *OOH involved in the OER (Figure 7d). It is interesting to note that no similar signals have been detected on the pristine MOF counterpart without the lattice strain effects. Combining operando SR-FTIR and operando XAS analyses, a close relationship between the Ni^{4+}/Ni^{2+} ratio and the IR signal intensity at ≈1050 cm^{-1} has been found, demonstrating the crucial catalytic role of high-valance Ni^{4+} in the lattice-strained MOF during the OER process (Figure 7e). This conclusion is further supported by another work reported by Yan and co-workers revealing the formation of key *OOH intermediates at the OER catalytic region using operando SR-FTIR characterization, which shows an emerging IR peak at 1030 cm^{-1} when the applied potential is greater than 1.4 V (versus RHE) during the OER (Figure 7f).[93]

Experimental evidence interpreting the OER reaction mechanism also comes from in situ SEIRA studies. In a recent work, Shao-Horn and co-workers have probed the formation of —OO group on a polycrystalline RuO_2 catalyst using this method.[16] The in situ SEIRA measurements demonstrate that a new peak at ≈899 cm^{-1} emerges when the applied potential reaches 1.5 V (versus RHE) or even higher, which can be successfully linked to the formation of proton-stabilized —OO species on the coordinatively-unsaturated Ru site that is stabilized by an adjacent —OH group on the neighboring sites (Figure 7g). DFT studies indicate that the removal of —OO, which is anchored by a hydrogen bond to an adjacent —OH group, from the RuO_2 (100) facet acts as the rate-determining step for the OER.

6.3. On-Line ICP-MS

The durability of OER electrocatalysts is significant toward the large-scale commercialization of sustainable energy-related devices. However, most of the OER electrocatalysts, no matter for noble metal-based materials working in the acidic electrolyte or non-noble metal-based catalysts performing in the alkaline solution, suffer greatly from metal dissolution due to the harsh operating conditions and hence lead to poor corrosion durability. Now, fortunately, on-line ICP-MS coupled with an electrochemical scanning flow cell (SFC) can serve as a powerful tool to enable the detection of the dissolved elements down to the ppt (part per trillion, 10^{-12}) level to study the performance decay mechanism of OER electrocatalysts. In situ generated liquid samples from the electrochemical SFC are directly introduced to the on-line ICP-MS instrument. The dissolved metal ions are analyzed simultaneously with the electrochemical reaction happening by compensating a short lag time (**Figure 8**a).[94] As an example, Geiger et al. have applied

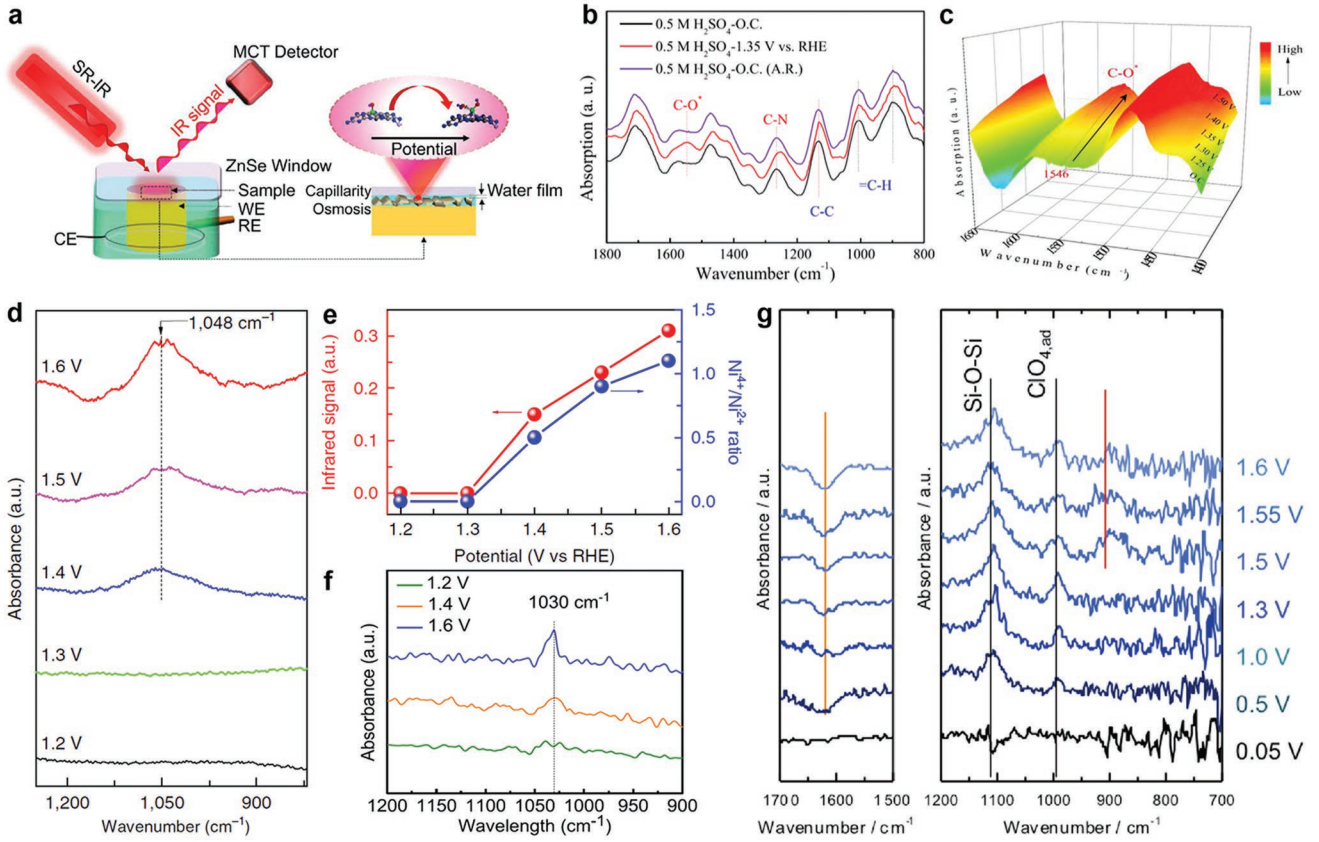

Figure 7. a) Schematic illustration of operando SR-IR setup. Reproduced with permission.[33] Copyright 2020, Elsevier. b,c) Operando SR-FTIR results of the amino-rich carbon material as a function of the applied potential. Reproduced with permission.[92] Copyright 2019, American Chemical Society. d) Operando SR-FTIR spectra of the lattice-strained NiFe-MOF under different potentials. e) Plots of the infrared signal at 1048 cm^{-1} and the Ni^{4+}/Ni^{2+} ratio at different potentials during the OER of NiFe-MOF catalyst. Reproduced with permission.[11] Copyright 2019, Nature Publishing Group. f) Operando SR-FTIR measurements of NiFe-MOF at different potentials. Reproduced with permission.[93] Copyright 2020, American Chemical Society. g) Operando SEIRA spectra for a polycrystalline RuO_2 surface at varying applied potentials. Reproduced with permission.[16] Copyright 2020, Nature Publishing Group.

the SFC-ICP-MS technique to study the degradation mechanism of an Ir-black catalyst by tracking the Ir dissolution in parallel with the electrochemical test.[95] A steady dissolution rate is detected during the first 2200-s chronopotentiometric operation. Meanwhile, the anodic potential gradually increases to maintain a constant current density. After 2200 s, the potential shows a sharp increase whereas the dissolution signal goes down to the baseline level (Figure 8b). The total amount of dissolved Ir can be converted into ≈1.3% of the overall Ir species printed on the working electrode, which rules out the possibility of catalyst detachment for this sharp potential increase. A reasonable explanation could be the increasing contact resistance at the catalyst film/backing interface. Importantly, one should pay attention to the pitfall that a steady electrochemical chronopotentiometric or chronoamperometric curve recorded during the stability test of the OER electrocatalysts cannot solely act as a meaningful evaluation criterion for the stability of the OER electrocatalysts. On-line ICP-MS measurements indicate that the active metal species keeps leaching during the chronopotentiometry test while showing a steady electrochemical performance output.[96] The dissolved metal ions would plague the membrane in the water electrolyzer and hence result in the overall performance decay.

6.4. APT

Besides the ability to measure the dissolved metal ions using on-line ICP-MS during the reaction, the microanalytical mass-spectroscopy technique of APT provides us an opportunity to map out the 3D distribution of chemical species with sub-nanometer spatial resolution, which is a powerful tool to track the structural evolution of OER electrocatalysts during the reaction.[97] For example, Mayrhofer and co-workers have probed the gradual structural transformation process from the pristine as-deposited Ir film to surface Ir oxide layers during the anodic oxidation reaction (Figure 8c).[71] The electrochemical oxide film prefers to grow at the grain boundaries, forming oxide islands with uneven distributions. The in situ gradually generated Ir oxide species with different oxidation state degrees as a function of the anodic oxidation operation time is found to be associated with a decreased activity but an improvement in stability

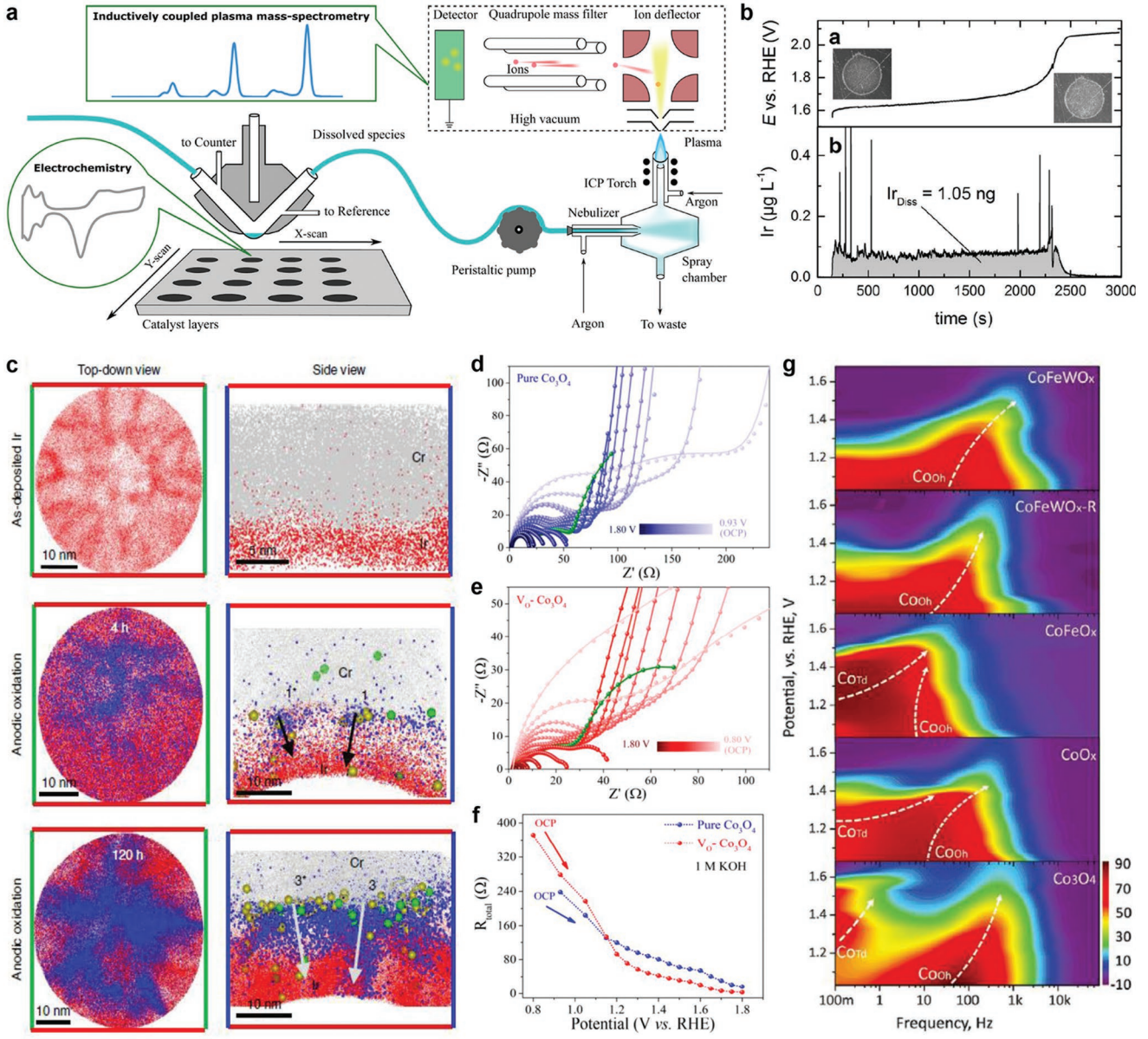

Figure 8. a) A schematic illustration of the SFC-ICP-MS setup. Reproduced with permission.[94] Copyright 2019, Wiley-VCH. b) Chronopotentiometric polarization curve and simultaneously recorded dissolution of Ir element as a function of the operation time for Ir-black catalyst. Reproduced with permission.[95] Copyright 2017, Wiley-VCH. c) Top-down and side views of APT reconstructions of as-deposited Ir film and in situ formed Ir oxides during the anodic oxidation process. Reproduced with permission.[71] Copyright 2018, Nature Publishing Group. Nyquist plots for d) pure Co_3O_4 and e) V_O-Co_3O_4 catalysts at different potentials. f) The R_{total} values as a function of the applied potential for two catalysts. Reproduced with permission.[27] Copyright 2020, American Chemical Society. g) Operando 2D contour Bode plots of different catalysts. Reproduced with permission.[98] Copyright 2020, Wiley-VCH.

toward the OER. This near-atomic resolution tomography technique helps advance the understanding of complex OER reaction mechanism between surface structure, oxidation state, and function in electrocatalysis.

6.5. EIS

EIS is a useful approach to probe the electrocatalytic reaction kinetics and the electrode/electrolyte interface properties. In a recent study, in situ EIS measurements have been performed by Wang and co-workers at different potentials in probing the OER reaction kinetics of pure Co_3O_4 and Co_3O_4 with oxygen vacancies (V_O-Co_3O_4).[27] The adsorption behavior of the intermediate *OH on the catalyst surface can be described by the *OH adsorption resistance (R_{CT}) and the pseudocapacitance. The results show that both pure Co_3O_4 and V_O-Co_3O_4 exhibit similar electrolyte resistivity values, whereas the total charge transfer resistance (R_{total}) is dominated by the R_{CT} values reflecting the ability to adsorb *OH species during the OER.

A lower R_{total} value is observed on the V_O-Co_3O_4 catalyst compared with the pure Co_3O_4, demonstrating the stronger ability to adsorb *OH, the reduced charge transfer resistance, and hence the facilitated OER reaction kinetics due to the presence of oxygen vacancy (Figure 8d–f). In another work, Chen et al. have applied in situ EIS to study the role of octahedral Co^{3+} site in an efficient $CoFeWO_x$ OER electrocatalyst.[98] The 2D contour Bode plots of different catalysts demonstrate a single-phase angle peak locus at 20×10^3 Hz for the $CoFeWO_x$ catalyst but the co-existence of octahedral and tetrahedron Co sites for $CoFeO_x$ and CoO_x, which agree well with the EXAFS analyses results (Figure 8g). The in situ EIS results coupled with other characterizations demonstrate that the octahedral Co^{3+} site serves as the primary OER active site for the $CoFeWO_x$ catalyst.

7. Theoretical Considerations

Theoretical calculations might be the best "in situ/operando" approach to study the reaction at the atomic/electronic scale. Here, the applied quotation mark is in consideration of some assumptions and approximations when building models, performing calculations, and analyzing data for the theoretical simulations, and hence is not completely reflecting the information of "under real working conditions." Nevertheless, theoretical simulations are still super powerful to provide us some pieces of essential information to predict, explain and guide experimental science. In this section, we would not spill much ink on the reaction mechanism discussions, but instead, focus on some parameters such as the solvent effect, applied potential, pH value with "in situ/operando" flavors.

7.1. Solvent Effect

Most DFT model calculations are based on the vacuum hypothesis, which misses lots of information on electrochemical reactions at the solid-liquid interface. Therefore, solvent effects involving both explicit and implicit considerations are crucial to be taken into account in the calculation processes. In electrochemical reactions such as the OER, the explicit solvent effect often is considered as the surface adsorbed or surrounding H_2O, OH, H^+, H_3O^+, and even K species. For example, Gauthier et al. studied the explicit solvent effect on the IrO_2 (110) model for the OER.[99] The inclusion of the explicit solvent greatly affects the geometry of adsorbed intermediates, however, but makes rather limited influence on the energetics of the reaction pathway (**Figure 9**a). One possible explanation is that the electrochemical reactions are mainly affected by catalyst-intermediate interactions, which are hard to be greatly influenced by the explicit solvent species. Notably, the solvent species may

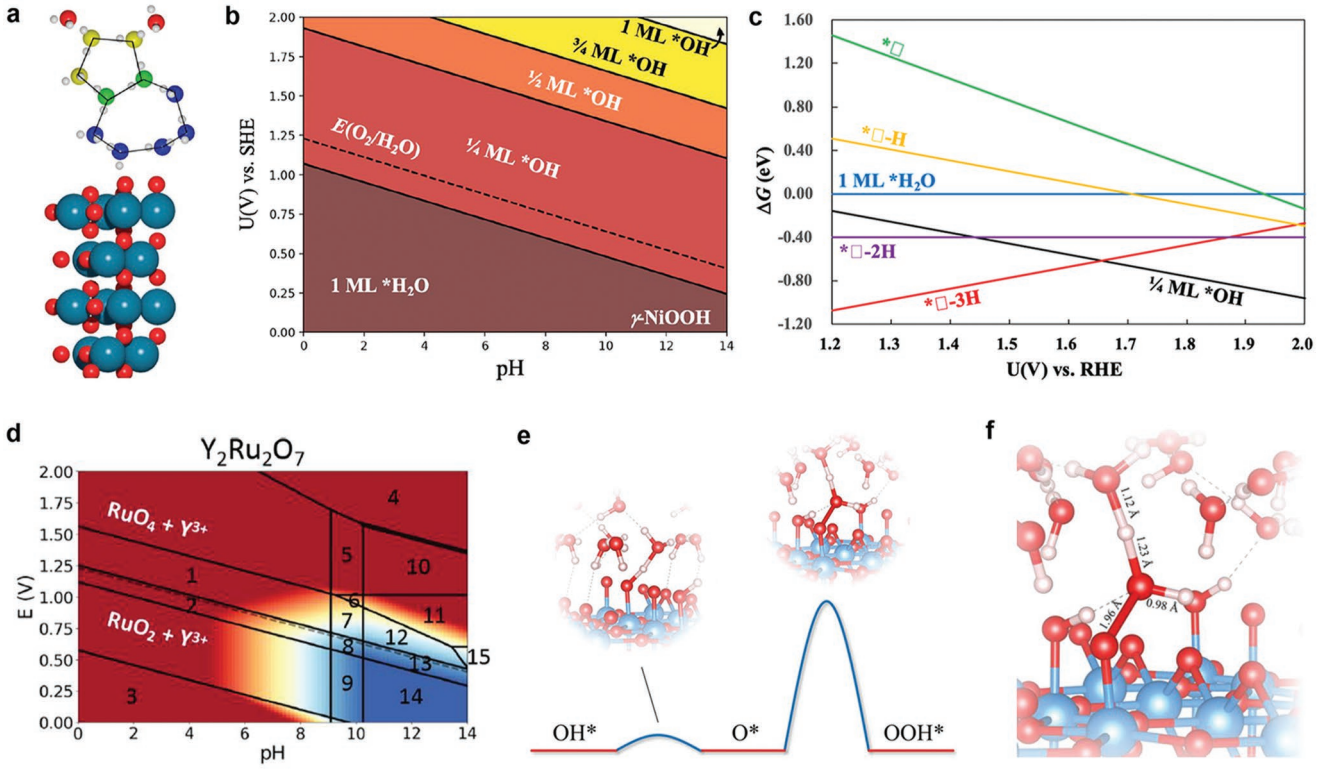

Figure 9. a) Model illustrating the solvent network on an IrO_2 [110] surface. Reproduced with permission.[99] Copyright 2019, American Chemical Society. b) Pourbaix diagram for the γ-NiOOH surface. c) Phase diagram of γ-NiOOH surfaces with different surface coverage. Reproduced with permission.[103] Copyright 2020, American Chemical Society. d) Pourbaix diagram for the $Y_2Ru_2O_7$ system. Reproduced with permission.[104] Copyright 2020, American Chemical Society. e) Schematic illustration of the reaction barriers of some elementary steps during the OER. f) The configuration of the transition state for *OOH formation on the IrO_2 [110] surface. Reproduced with permission.[22] Copyright 2019, American Chemical Society.

take part in the reactions directly and hence change the reaction pathways.[100,101] The implicit solvent effect has also been considered by the inclusion of the dielectric constant of the solvent.[102] Currently, the role of the solvent is still not quite clear in theoretically studying the OER. Therefore, future calculation works should carefully consider the solvent effect on the reactions.

7.2. Applied Potential and pH Value

It is well known that the applied electrochemical potential and the pH values of the solvent will alter the surface state of catalyst and hence affect the OER activity. Besides the thermodynamic considerations of the free energies at different potentials, theoretical calculations are also able to study the surface structure of catalysts under different potentials and pH values. For instance, Liu and co-workers have constructed the surface Pourbaix diagram from the DFT thermodynamics based on a γ-NiOOH surface model.[103] With an applied potential, the adsorbed $*H_2O$ may decompose to *OH. A higher applied potential is associated with a higher degree of *OH coverage on the surface (Figure 9b). The location of the Ni vacancy on the defective γ-NiOOH surface can also be thermodynamically determined by the phase diagram considering the free energies as the function of the applied potentials (Figure 9c). The *□-3H phase (catalyst adsorbed with 3 H) is demonstrated as the most stable configuration under OER conditions (< 1.65 V versus RHE), indicating that the applied potentials cause instability of the dangling O atoms on the NiOOH catalyst surface. Therefore, the unsaturated O atoms will capture protons from the electrolyte. Another example involves a study of the thermodynamic stability of metal-doped RuO_2 OER catalysts.[104] Pourbaix diagrams are constructed from the DFT calculated free energies at different electrochemical potentials and pH values in aqueous conditions (Figure 9d). At the OER catalytic region in acidic conditions, the most stable states of the doped metal species are aqueous ions while the most stable state of Ru is RuO_4, indicating that all materials will ultimately dissolve into the electrolyte during the OER. The significant thermodynamic driving force to induce the leaching of metallic species agrees well with the experimental observations.

7.3. Reaction Barrier

For electrochemical OER, DFT theoretical calculations usually only consider the thermodynamics factors of the reaction pathway involving adsorbed *OH, *O, and *OOH as key intermediates in the adsorbate evolution mechanism, or the lattice oxygen oxidation mechanism which involves direct O—O bond coupling.[55] However, the reaction kinetics of the OER has seldom been considered due to the complexity when performing the calculation and the high computational cost. The reaction barriers as computed by the transition state search method are of great significance when evaluating the catalytic activity of OER catalysts. Recently, Nørskov and co-workers evaluated the OER kinetics of a couple of rutile materials via calculating the reaction barriers on an explicit model.[22] The reaction kinetics of proton transfer between oxygen atoms in the electrolyte and at the catalyst surface is facile with a negligible reaction barrier (Figure 9e). However, the O—O bond formation step, that is, the formation of *OOH, shows a much higher reaction barrier, and hence acts as the most likely rate-determining step in all catalysts (Figure 9f). In another example, Wu et al. have performed DFT simulations on the reaction barriers of some key elementary steps on some pure metal and alloy models, demonstrating the facilitated reaction kinetics on the alloy oxygen electrocatalysts due to the catalytic synergy.[78] It is worth noting that the overpotentials derived from DFT calculations without reaction kinetics considerations are often underestimated.

8. Conclusions and Perspectives

The last decades have witnessed the successful and wide applications of in situ/operando techniques with a deep penetration into electrochemical OER studies. The advantages and limitations of some commonly used in situ/operando characterization approaches with elaborated examples have been demonstrated in this review. To summarize briefly, the current research advances of TEM/STEM techniques, which offer us opportunities to observe the morphology and composition changes during the reaction, are largely based on ex situ characterizations. A number of works have been reported by using ex situ high resolution TEM/STEM to demonstrate the formation of metal oxyhydroxide structure after the OER catalysis. The demand of the ultra-high vacuum condition, the difficulty in the design of in situ TEM cell, and the possible damage from the electron beam to the catalysts are existing challenges for the development of operando TEM techniques. Operando XAS technique has received tremendous research attention on OER studies recently. Specifically, Operando EXAFS is able to capture and analyze the coordination environment of atoms in the catalysts during the reaction, while XANES and soft XAS methodologies can provide information about the electronic structure of catalysts. Interestingly, that most operando XAS studies arrive at similar conclusions that the structure of the non-noble metal-based OER pre-catalysts will transform to the metal oxyhydroxide structure and the valence state of the catalytically active species will increase during the reaction under the applied electrochemical potential at the OER catalytic region. However, XAS is a bulk detection technique by measuring the ensemble catalyst film and hence cannot specifically reflect the structure information of the catalytic reaction occurring at the surface/subsurface region of catalysts or at the solid-liquid interface. Surface-sensitive XPS characterizations, especially for the in situ APXPS technique, can probe the electronic structural evolution of catalysts and demonstrate valence state changes of elements during the OER. The results often agree well with the operando XANES analyses with increased oxidation states of the catalytically active metals, indicating the structural transformation from the pre-catalysts to M-OOH structures. Operando XRD technique has been well developed but is usually unable to capture the reconstruction process of the OER catalysts due to the low crystallinities of the materials. Fortunately, operando HE-XRD and the corresponding simulation and analyzing techniques serve as the potential promising approaches to study the

dynamic structural evolution of OER electrocatalysts. In situ Raman and IR optical spectroscopies are also capable to substantiate the formation of M-OOH structure and detect other O-containing species during the OER catalysis. However, most in situ Raman studies can only prove the formation of Ni-OOH but is not good at probing other metals such as Fe-OOH. The in situ/operando IR characterizations still need more systematic works to build a more comprehensive database as references. The above in situ/operando characterizations all demonstrate the formation of or the structural evolution to M-OOH species, acting as the OER catalytically active phase for non-noble metal-based OER electrocatalysts, and surface amorphization often happens for all OER electrocatalysts. Moreover, the catalyst degradation mechanism and stability studies by measuring the metal dissolution using on-line ICP-MS can provide constructive information toward the commercialization of OER catalysts in practical devices, where the membrane can be easily plagued by the dissolved metal cations especially for non-noble metal-based OER electrocatalysts. Theoretical DFT calculation is a powerful tool to understand the reaction energetics, while it is challenged by the total and precise reflection of the real working condition of catalysis. Other in situ/operando characterizations such as APT, EIS, Mössbauer spectroscopy, X-ray emission spectroscopy, differential electrochemical mass spectrometry, electrochemical quartz crystal balance, etc. can also assist the study of OER electrocatalysts, but we will not elaborate them in detail in this review.

Although impressive research progresses have been achieved in the field of in situ/operando characterizations, we have to say that we are still facing an unsatisfactory status with a lack of efficient OER electrocatalysts for the large-scale commercialization and unsolved puzzles regarding the OER reaction mechanisms. We provide here the following perspectives and possible strategies to address the current bottlenecks in OER electrocatalysts, and hope to witness the future research and industrial progress on OER-related applications involving water electrolyzers, CO_2 electrolyzers, nitrogen reduction cells, metal-air batteries, reversible fuel cells, among others.

1) Integrate multiple in situ/operando techniques. Since the individual in situ/operando technique can only provide limited information about the catalytic reaction from specific but different aspects, therefore, a close combination of multiple in situ/operando characterizations is expected to obtain a more comprehensive picture of the catalytic reaction. For example, the cooperation of in situ/operando XAS, Raman, and IR spectroscopies on the same in situ/operando reaction cell using synchrotron light sources will offer us the simultaneous detections of the catalyst structure change and the reaction intermediate evolution during the OER operation. This can enable a more convincing mechanism study at the same temporal and spatial scale.
2) Bridge the gap between in situ/operando cells and the real working devices. Currently, one major challenge of operando experiments is the design of the cell and its components. Generally, the operando cells are built upon the requirements of specific operando characterization testing conditions. To satisfy the operando investigation condition, the reaction cells are often designed in distorted configurations, resulting in the mismatch between the operando conditions and real working status. The possible damage of the catalyst structure from the strong X-rays and electron beams makes the situation more complicated. Considering the above factors, the collected information may not fully reflect the true catalytic reaction. Therefore, developing and optimizing real electrolyzers which can truly bridge the gap between operando testing and real working condition with less device structure change and minimal system damage are challenging but urgently necessary.
3) Get more precisely time-resolved in situ/operando characterizations to capture the dynamic structural evolution. At present, it is still challenging to conduct real and precise time-resolved operando characterizations to capture the dynamic structure changes of OER electrocatalysts. Current evidence from operando measurements usually needs a certain period of time to collect the results. For example, it takes a couple of minutes to collect one XAS or XRD spectrum. In fact, the lifetime of reaction intermediates is often at the picosecond level and most importantly the structure of catalyst will definitely experience a significant and often irreversible change during the time to collect one spectrum, especially at the initial reaction stage where the catalyst surface reconstruction happens very quickly. Further advancement, for example, using fast scan technologies (capturing one XAS spectrum about or within ten seconds) and X-rays with high energies (collecting one XRD pattern within a few seconds without sacrificing the data quality) of operando characterizations to improve the temporal resolution are expected to tackle the current drawbacks of operando techniques. Furthermore, high spatial resolution and energy resolution will benefit the capturing of the subtle dynamic structural evolution of catalysts. For example, as for some reaction systems, the differences in the XAFS spectra are slightly influenced by the presence of various adsorbates, which makes it difficult to capture the detailed differences in the electronic and coordination structures extracted from XAFSs. Higher energy resolution and spatial resolution are required to study catalysis systems with small variations.
4) Develop other surface sensitive techniques. Currently, there are some surface-sensitive techniques that already have been applied in OER studies. For example, XPS can determine the electronic structure of surface species of the catalysts, and FTIR and Raman spectroscopies can provide the structural information at the solid-liquid interface. Besides, surface structure information can also be obtained using XAFS techniques. For example, manipulating the depth of X-ray penetration of the target samples, such as applying grazing incidence XAFS technique, can extract the surface structure information of materials. In addition, applying differential EXAFS, which is the difference between two conventional EAXFS spectra, during the data processing can capture the atomic perturbation happening at the catalytic surface region.
5) Design and fabricate model catalysts suitable for operando analyses. The electrocatalytic OER happening at the solid-liquid interface is very complex. The diversity of different bulk or local composition, crystal or amorphous structure, facet, particle size, and among others make the situation even worse. On this occasion, it is often hard to accurately and

efficiently extract the dominant factor which is controlling and influencing the catalytic reaction. The design and successful fabrication of model catalysts with controlled size, shape, surface facet, composition, and phase structure for operando characterizations will help make the story simpler and get more convincing analyses and results. In addition, as the structural evolution of OER electrocatalysts mainly occurs at the surface/subsurface region of the catalytic materials, the fabrication of ultrathin nanosheet/nanofilm and thin-walled hollow structures can help concentrate the chemical reaction active sites to be more easily accessible for operando detections. This strategy is very suitable for bulk detection techniques by collecting the structure information of the ensemble materials, such as XAS and XRD.

6) Apply isotope labeling experiments to assist the reaction mechanism studies. The detection and substantiation of the formation of M—OOH species during or after the OER conditioning have been widely reported in the literature using a wide range of in situ/operando techniques, such as TEM, XAS, XPS, XRD, Raman, IR, etc. However, the detailed reaction mechanism regarding the reaction pathway of how the OER occurs remains elusive. The participation of lattice oxygen and the role of oxygen vacancy in the catalysts, which are crucial in the reaction, need further demonstrations. Isotope labeling experiments are hence encouraged to be involved in the operando characterizations to obtain better fundamental understandings of the OER reaction mechanism.
7) Combine operando experimental investigations with theoretical calculations. Operando experimental evidence is the most straightforward and convincing data on OER electrocatalyst studies, but it often lacks capability to obtain the reaction information from the aspect of catalyst-intermediate interactions at the atomic or even electronic level. Fortunately, theoretical simulations are powerful approaches to predict, elucidate, and understand the experimental results. The successful detections of the evolution of key intermediates and the structural evolution of reactive centers, as well as the role of ions and electrolytes can be reflected in theoretical calculation models. With particular attention, machine learning should receive more research attention in accelerating the prediction and screening of better OER electrocatalysts toward efficient catalyst designs and fabrications in experiments. Through the high-throughput calculation of some key descriptors such as adsorption energies, d-band center, and coordination number by well-constructed machine learning model, the reaction thermodynamics, reaction kinetics, reaction pathways, rate-determining steps, and possible strategies to guide the catalyst optimization and evolution can be output from a close combination of operando experiments and theoretical calculations.

Acknowledgements

S.Z. and Z.-P.W. contributed equally to this work. This work received financial support from the King Abdullah University of Science and Technology (KAUST). X.W.L. acknowledges the funding support from the Ministry of Education of Singapore through the Academic Research Fund (AcRF) Tier-2 grant (MOE2019-T2-2-049).

Conflict of Interest

The authors declare no conflict of interest.

Keywords

electrocatalysts, operando reaction, oxygen evolution reaction, reaction mechanism, structural evolution

Received: October 30, 2021
Revised: December 8, 2021
Published online: January 5, 2022

[1] J. Kibsgaard, I. Chorkendorff, *Nat. Energy* **2019**, *4*, 430.
[2] Z. W. Seh, J. Kibsgaard, C. F. Dickens, I. Chorkendorff, J. K. Nørskov, T. F. Jaramilo, *Science* **2017**, *355*, eaad4998.
[3] Z. Yan, J. L. Hitt, J. A. Turner, T. E. Mallouk, *Proc. Natl. Acad. Sci. USA* **2020**, *117*, 12558.
[4] R. C. Armstrong, C. Wolfram, K. P. de Jong, R. Gross, N. S. Lewis, B. Boardman, A. J. Ragauskas, K. Ehrhardt-Martinez, G. Crabtree, M. V. Ramana, *Nat. Energy* **2016**, *1*, 15020.
[5] L. C. Seitz, C. F. Dickens, K. Nishio, Y. Hikita, J. Montoya, A. Doyle, C. Kirk, A. Vojvodic, H. Y. Hwang, J. K. Norskov, T. F. Jaramillo, *Science* **2016**, *353*, 1011.
[6] Z. P. Wu, X. F. Lu, S. Q. Zang, X. W. Lou, *Adv. Funct. Mater.* **2020**, *30*, 1910274.
[7] D. Y. Chung, P. P. Lopes, P. Farinazzo Bergamo Dias Martins, H. He, T. Kawaguchi, P. Zapol, H. You, D. Tripkovic, D. Strmcnik, Y. Zhu, S. Seifert, S. Lee, V. R. Stamenkovic, N. M. Markovic, *Nat. Energy* **2020**, *5*, 222.
[8] S. L. Zhang, B. Y. Guan, X. F. Lu, S. Xi, Y. Du, X. W. Lou, *Adv. Mater.* **2020**, *32*, 2002235.
[9] J. Zhang, L. Yu, Y. Chen, X. F. Lu, S. Gao, X. W. Lou, *Adv. Mater.* **2020**, *32*, 1906432.
[10] Z. P. Wu, H. Zhang, S. Zuo, Y. Wang, S. L. Zhang, J. Zhang, S. Q. Zang, X. W. Lou, *Adv. Mater.* **2021**, *33*, 2103004.
[11] W. Cheng, X. Zhao, H. Su, F. Tang, W. Che, H. Zhang, Q. Liu, *Nat. Energy* **2019**, *4*, 115.
[12] Y. Sun, H. Liao, J. Wang, B. Chen, S. Sun, S. J. H. Ong, S. Xi, C. Diao, Y. Du, J. O. Wang, M. B. H. Breese, S. Li, H. Zhang, Z. J. Xu, *Nat. Catal.* **2020**, *3*, 554.
[13] S. Zhao, C. Tan, C.-T. He, P. An, F. Xie, S. Jiang, Y. Zhu, K.-H. Wu, B. Zhang, H. Li, J. Zhang, Y. Chen, S. Liu, J. Dong, Z. Tang, *Nat. Energy* **2020**, *5*, 881.
[14] T. Wu, S. Sun, J. Song, S. Xi, Y. Du, B. Chen, W. A. Sasangka, H. Liao, C. L. Gan, G. G. Scherer, L. Zeng, H. Wang, H. Li, A. Grimaud, Z. J. Xu, *Nat. Catal.* **2019**, *2*, 763.
[15] Y. Zhu, J. Wang, H. Chu, Y. C. Chu, H. M. Chen, *ACS Energy Lett.* **2020**, *5*, 1281.
[16] R. R. Rao, M. J. Kolb, L. Giordano, A. F. Pedersen, Y. Katayama, J. Hwang, A. Mehta, H. You, J. R. Lunger, H. Zhou, N. B. Halck, T. Vegge, I. Chorkendorff, I. E. L. Stephens, Y. Shao-Horn, *Nat. Catal.* **2020**, *3*, 516.
[17] J. Song, C. Wei, Z. F. Huang, C. Liu, L. Zeng, X. Wang, Z. J. Xu, *Chem. Soc. Rev.* **2020**, *49*, 2196.
[18] S. Li, Y. Gao, N. Li, L. Ge, X. Bu, P. Feng, *Energy Environ. Sci.* **2021**, *14*, 1897.
[19] L. Gao, X. Cui, C. D. Sewell, J. Li, Z. Lin, *Chem. Soc. Rev.* **2021**, *50*, 8428.
[20] D. Zhou, P. Li, X. Lin, A. McKinley, Y. Kuang, W. Liu, W. F. Lin, X. Sun, X. Duan, *Chem. Soc. Rev.* **2021**, *50*, 8790.
[21] Z. F. Huang, J. Song, S. Dou, X. Li, J. Wang, X. Wang, *Matter* **2019**, *1*, 1494.

[22] C. F. Dickens, C. Kirk, J. K. Nørskov, *J. Phys. Chem. C* **2019**, *123*, 18960.
[23] H. Xiao, H. Shin, W. A. Goddard III, *Proc. Natl. Acad. Sci. USA* **2018**, *115*, 5872.
[24] X. Xu, F. Song, X. Hu, *Nat. Commun.* **2016**, *7*, 12324.
[25] H. Zhang, W. Zhou, J. Dong, X. F. Lu, X. W. Lou, *Energy Environ. Sci.* **2019**, *12*, 3348.
[26] J. Nai, Y. Lu, L. Yu, X. Wang, X. W. Lou, *Adv. Mater.* **2017**, *29*, 1703870.
[27] Z. Xiao, Y. C. Huang, C. L. Dong, C. Xie, Z. Liu, S. Du, W. Chen, D. Yan, L. Tao, Z. Shu, G. Zhang, H. Duan, Y. Wang, Y. Zou, R. Chen, S. Wang, *J. Am. Chem. Soc.* **2020**, *142*, 12087.
[28] M. A. Bañares, *Catal. Today* **2005**, *100*, 71.
[29] J. Li, J. Gong, *Energy Environ. Sci.* **2020**, *13*, 3748.
[30] J. Timoshenko, B. R. Cuenya, *Chem. Rev.* **2021**, *121*, 882.
[31] Y. Yang, Y. Xiong, R. Zeng, X. F. Lu, M. Krumov, X. Huang, W. Xu, H. Wang, F. J. DiSalvo, J. D. Brock, D. A. Muller, H. D. Abruña, *ACS Catal.* **2021**, *11*, 1136.
[32] A. D. Handoko, F. Wei, B. S. Y. Jenndy, Z. W. Seh, *Nat. Catal.* **2018**, *1*, 922.
[33] Y. Li, W. Cheng, H. Su, X. Zhao, J. He, Q. Liu, *Nano Energy* **2020**, *77*, 105121.
[34] D. Zhang, Y. Zhu, L. Liu, X. Ying, C. E. Hsiung, R. Sougrat, K. Li, Y. Han, *Science* **2018**, *359*, 675.
[35] J. Park, H. Zhao, S. D. Kang, K. Lim, C. C. Chen, Y. S. Yu, R. D. Braatz, D. A. Shapiro, J. Hong, M. F. Toney, M. Z. Bazant, W. C. Chueh, *Nat. Mater.* **2021**, *20*, 991.
[36] J. Shan, C. Ye, S. Chen, T. Sun, Y. Jiao, L. Liu, C. Zhu, L. Song, Y. Han, M. Jaroniec, Y. Zhu, Y. Zheng, S. Z. Qiao, *J. Am. Chem. Soc.* **2021**, *143*, 5201.
[37] P. P. Lopes, D. Y. Chung, X. Rui, H. Zheng, H. He, P. Farinazzo Bergamo Dias Martins, D. Strmcnik, V. R. Stamenkovic, P. Zapol, J. F. Mitchell, R. F. Klie, N. M. Markovic, *J. Am. Chem. Soc.* **2021**, *143*, 2741.
[38] A. Grimaud, A. Demortière, M. Saubanère, W. Dachraoui, M. Duchamp, M. L. Doublet, J. M. Tarascon, *Nat. Energy* **2017**, *2*, 16189.
[39] D. Gohl, A. Garg, P. Paciok, K. J. J. Mayrhofer, M. Heggen, Y. Shao-Horn, R. E. Dunin-Borkowski, Y. Roman-Leshkov, M. Ledendecker, *Nat. Mater.* **2020**, *19*, 287.
[40] T. H. Shen, L. Spillane, J. Vavra, T. H. M. Pham, J. Peng, Y. Shao-Horn, V. Tileli, *J. Am. Chem. Soc.* **2020**, *142*, 15876.
[41] N. Hodnik, G. Dehm, K. J. Mayrhofer, *Acc. Chem. Res.* **2016**, *49*, 2015.
[42] G. Wan, J. W. Freeland, J. Kloppenburg, G. Petretto, J. N. Nelson, D. Y. Kuo, C. J. Sun, J. Wen, J. T. Diulus, G. S. Herman, Y. Dong, R. Kou, J. Sun, S. Chen, K. M. Shen, D. G. Schlom, G. M. Rignanese, G. Hautier, D. D. Fong, Z. Feng, H. Zhou, J. Suntivich, *Sci. Adv.* **2021**, *7*, eabc7323.
[43] E. Fabbri, D. F. Abbott, M. Nachtegaal, T. J. Schmidt, *Curr. Opin. Electrochem.* **2017**, *5*, 20.
[44] Z. Sun, Q. Liu, T. Yao, W. Yan, S. Wei, *Sci. China Mater.* **2015**, *58*, 313.
[45] L. J. Enman, M. B. Stevens, M. H. Dahan, M. R. Nellist, M. C. Toroker, S. W. Boettcher, *Angew. Chem., Int. Ed.* **2018**, *57*, 12840.
[46] H. N. Nong, L. J. Falling, A. Bergmann, M. Klingenhof, H. P. Tran, C. Spori, R. Mom, J. Timoshenko, G. Zichittella, A. Knop-Gericke, S. Piccinin, J. Perez-Ramirez, B. R. Cuenya, R. Schlogl, P. Strasser, D. Teschner, T. E. Jones, *Nature* **2020**, *587*, 408.
[47] S. C. Lin, C. C. Chang, S. Y. Chiu, H. T. Pai, T. Y. Liao, C. S. Hsu, W. H. Chiang, M. K. Tsai, H. M. Chen, *Nat. Commun.* **2020**, *11*, 3525.
[48] H. Zhang, P. An, W. Zhou, B. Y. Guan, P. Zhang, J. Dong, X. W. Lou, *Sci. Adv.* **2018**, *4*, eaao6657.
[49] H. Zhang, S. Zuo, M. Qiu, S. Wang, Y. Zhang, J. Zhang, X. W. Lou, *Sci. Adv.* **2020**, *6*, eabb9823.
[50] X. Wang, H. Xiao, A. Li, Z. Li, S. Liu, Q. Zhang, Y. Gong, L. Zheng, Y. Zhu, C. Chen, D. Wang, Q. Peng, L. Gu, X. Han, J. Li, Y. Li, *J. Am. Chem. Soc.* **2018**, *140*, 15336.
[51] Y. Huang, S. L. Zhang, X. F. Lu, Z. P. Wu, D. Luan, X. W. Lou, *Angew. Chem., Int. Ed.* **2021**, *60*, 11841.
[52] B. Y. Xia, Y. Yan, H. B. Wu, X. W. Lou, X. Wang, *Nat. Energy* **2016**, *1*, 15006.
[53] X. Su, Y. Wang, J. Zhou, S. Gu, J. Li, S. Zhang, *J. Am. Chem. Soc.* **2018**, *140*, 11286.
[54] F. Dionigi, Z. Zeng, I. Sinev, T. Merzdorf, S. Deshpande, M. B. Lopez, S. Kunze, I. Zegkinoglou, H. Sarodnik, D. Fan, A. Bergmann, J. Drnec, J. F. Araujo, M. Gliech, D. Teschner, J. Zhu, W. X. Li, J. Greeley, B. R. Cuenya, P. Strasser, *Nat. Commun.* **2020**, *11*, 2522.
[55] Z.-F. Huang, J. Song, Y. Du, S. Xi, S. Dou, J. M. V. Nsanzimana, C. Wang, Z. J. Xu, X. Wang, *Nat. Energy* **2019**, *4*, 329.
[56] T. Wang, G. Nam, Y. Jin, X. Wang, P. Ren, M. G. Kim, J. Liang, X. Wen, H. Jang, J. Han, Y. Huang, Q. Li, J. Cho, *Adv. Mater.* **2018**, *30*, 1800757.
[57] C. Kuai, Z. Xu, C. Xi, A. Hu, Z. Yang, Y. Zhang, C. J. Sun, L. Li, D. Sokaras, C. Dong, S. Z. Qiao, X. W. Du, F. Lin, *Nat. Catal.* **2020**, *3*, 743.
[58] D. Friebel, M. W. Louie, M. Bajdich, K. E. Sanwald, Y. Cai, A. M. Wise, M. J. Cheng, D. Sokaras, T. C. Weng, R. Alonso-Mori, R. C. Davis, J. R. Bargar, J. K. Norskov, A. Nilsson, A. T. Bell, *J. Am. Chem. Soc.* **2015**, *137*, 1305.
[59] R. Subbaraman, D. Tripkovic, K. C. Chang, D. Strmcnik, A. P. Paulikas, P. Hirunsit, M. Chan, J. Greeley, V. Stamenkovic, N. M. Markovic, *Nat. Mater.* **2012**, *11*, 550.
[60] B. Zhang, L. Wang, Z. Cao, S. M. Kozlov, F. P. García de Arquer, C. T. Dinh, J. Li, Z. Wang, X. Zheng, L. Zhang, Y. Wen, O. Voznyy, R. Comin, P. De Luna, T. Regier, W. Bi, E. E. Alp, C.-W. Pao, L. Zheng, Y. Hu, Y. Ji, Y. Li, Y. Zhang, L. Cavallo, H. Peng, E. H. Sargent, *Nat. Catal.* **2020**, *3*, 985.
[61] S. Lee, K. Banjac, M. Lingenfelder, X. Hu, *Angew. Chem., Int. Ed.* **2019**, *58*, 10295.
[62] J. H. Choy, D. K. Kim, S. H. Hwang, G. Demazeau, D. Y. Jung, *J. Am. Chem. Soc.* **1995**, *117*, 8557.
[63] K. Jiang, M. Luo, M. Peng, Y. Yu, Y. R. Lu, T. S. Chan, P. Liu, F. M. F. de Groot, Y. Tan, *Nat. Commun.* **2020**, *11*, 2701.
[64] L. Li, H. Sun, Z. Hu, J. Zhou, Y. C. Huang, H. Huang, S. Song, C. W. Pao, Y. C. Chang, A. C. Komarek, H. J. Lin, C. T. Chen, C. L. Dong, J. Q. Wang, L. Zhang, *Adv. Funct. Mater.* **2021**, *31*, 2104746.
[65] W. Wan, Y. Zhao, S. Wei, C. A. Triana, J. Li, A. Arcifa, C. S. Allen, R. Cao, G. R. Patzke, *Nat. Commun.* **2021**, *12*, 5589.
[66] X. Zheng, J. Tang, A. Gallo, J. A. Garrido Torres, X. Yu, C. J. Athanitis, E. M. Been, P. Ercius, H. Mao, S. C. Fakra, C. Song, R. C. Davis, J. A. Reimer, J. Vinson, M. Bajdich, Y. Cui, *Proc. Natl. Acad. Sci. USA* **2021**, *118*, e2101817118.
[67] J. W. Smith, R. J. Saykally, *Chem. Rev.* **2017**, *117*, 13909.
[68] X. Zheng, B. Zhang, P. De Luna, Y. Liang, R. Comin, O. Voznyy, L. Han, F. P. Garcia de Arquer, M. Liu, C. T. Dinh, T. Regier, J. J. Dynes, S. He, H. L. Xin, H. Peng, D. Prendergast, X. Du, E. H. Sargent, *Nat. Chem.* **2018**, *10*, 149.
[69] B. Zhang, X. Zheng, O. Voznyy, R. Comin, M. Bajdich, M. García-Melchor, L. Han, J. Xu, M. Liu, L. Zheng, F. P. García de Arquer, C. T. Dinh, F. Fan, M. Yuan, E. Yassitepe, N. Chen, T. Regier, P. Liu, Y. Li, P. D. Luna, A. Janmohamed, H. L. Xin, H. Yang, A. Vojvodic, E. H. Sargent, *Science* **2016**, *352*, 333.
[70] L. Nguyen, F. F. Tao, Y. Tang, J. Dou, X. J. Bao, *Chem. Rev.* **2019**, *119*, 6822.
[71] T. Li, O. Kasian, S. Cherevko, S. Zhang, S. Geiger, C. Scheu, P. Felfer, D. Raabe, B. Gault, K. J. J. Mayrhofer, *Nat. Catal.* **2018**, *1*, 300.

[72] Y. Han, H. Zhang, Y. Yu, Z. Liu, *ACS Catal.* **2021**, *11*, 1464.
[73] M. Favaro, W. S. Drisdell, M. A. Marcus, J. M. Gregoire, E. J. Crumlin, J. A. Haber, J. Yano, *ACS Catal.* **2016**, *7*, 1248.
[74] M. Favaro, J. Yang, S. Nappini, E. Magnano, F. M. Toma, E. J. Crumlin, J. Yano, I. D. Sharp, *J. Am. Chem. Soc.* **2017**, *139*, 8960.
[75] J. Conder, R. Bouchet, S. Trabesinger, C. Marino, L. Gubler, C. Villevieille, *Nat. Energy* **2017**, *2*, 17069.
[76] Z. Yan, H. Sun, X. Chen, H. Liu, Y. Zhao, H. Li, W. Xie, F. Cheng, J. Chen, *Nat. Commun.* **2018**, *9*, 2373.
[77] C. S. Hsu, N. T. Suen, Y. Y. Hsu, H. Y. Lin, C. W. Tung, Y. F. Liao, T. S. Chan, H. S. Sheu, S. Y. Chen, H. M. Chen, *Phys. Chem. Chem. Phys.* **2017**, *19*, 8681.
[78] Z. P. Wu, D. T. Caracciolo, Y. Maswadeh, J. Wen, Z. Kong, S. Shan, J. A. Vargas, S. Yan, E. Hopkins, K. Park, A. Sharma, Y. Ren, V. Petkov, L. Wang, C. J. Zhong, *Nat. Commun.* **2021**, *12*, 859.
[79] Z. P. Wu, S. Shan, S. Q. Zang, C. J. Zhong, *Acc. Chem. Res.* **2020**, *53*, 2913.
[80] J. T. Mefford, A. R. Akbashev, M. Kang, C. L. Bentley, W. E. Gent, H. D. Deng, D. H. Alsem, Y. S. Yu, N. J. Salmon, D. A. Shapiro, P. R. Unwin, W. C. Chueh, *Nature* **2021**, *593*, 67.
[81] C. Hess, *Chem. Soc. Rev.* **2021**, *50*, 3519.
[82] H. Zhang, C. Wang, H. L. Sun, G. Fu, S. Chen, Y. J. Zhang, B. H. Chen, J. R. Anema, Z. L. Yang, J. F. Li, Z. Q. Tian, *Nat. Commun.* **2017**, *8*, 15447.
[83] N. Chen, T. H. Xiao, Z. Luo, Y. Kitahama, K. Hiramatsu, N. Kishimoto, T. Itoh, Z. Cheng, K. Goda, *Nat. Commun.* **2020**, *11*, 4772.
[84] R. Zhang, Y. Zhang, Z. C. Dong, S. Jiang, C. Zhang, L. G. Chen, L. Zhang, Y. Liao, J. Aizpurua, Y. Luo, J. L. Yang, J. G. Hou, *Nature* **2013**, *498*, 82.
[85] K. H. Cho, S. Park, H. Seo, S. Choi, M. Y. Lee, C. Ko, K. T. Nam, *Angew. Chem., Int. Ed.* **2021**, *60*, 4673.
[86] X. Bo, R. K. Hocking, S. Zhou, Y. Li, X. Chen, J. Zhuang, Y. Du, C. Zhao, *Energy Environ. Sci.* **2020**, *13*, 4225.
[87] L. Gao, X. Cui, Z. Wang, C. D. Sewell, Z. Li, S. Liang, M. Zhang, J. Li, Y. Hu, Z. Lin, *Proc. Natl. Acad. Sci. USA* **2021**, *118*, e2023421118.
[88] J. Huang, Y. Li, Y. Zhang, G. Rao, C. Wu, Y. Hu, X. Wang, R. Lu, Y. Li, J. Xiong, *Angew. Chem., Int. Ed.* **2019**, *58*, 17458.
[89] H. S. Ahn, A. J. Bard, *J. Am. Chem. Soc.* **2016**, *138*, 313.
[90] J. C. Dong, X. G. Zhang, V. Briega-Martos, X. Jin, S. Chen, Z. L. Yang, D. Y. Wu, J. M. Feliu, C. T. Williams, Z. Q. Tian, J. F. Li, *Nat. Energy* **2019**, *4*, 60.
[91] S. Zhu, X. Qin, Y. Yao, M. Shao, *J. Am. Chem. Soc.* **2020**, *142*, 8748.
[92] X. Zhao, H. Su, W. Cheng, H. Zhang, W. Che, F. Tang, Q. Liu, *ACS Appl. Mater. Interfaces* **2019**, *11*, 34854.
[93] Q. Ji, Y. Kong, C. Wang, H. Tan, H. Duan, W. Hu, G. Li, Y. Lu, N. Li, Y. Wang, J. Tian, Z. Qi, Z. Sun, F. Hu, W. Yan, *ACS Catal.* **2020**, *10*, 5691.
[94] O. Kasian, S. Geiger, K. J. J. Mayrhofer, S. Cherevko, *Chem. Rec.* **2019**, *19*, 2130.
[95] S. Geiger, O. Kasian, A. M. Mingers, S. S. Nickey, K. Haenen, K. J. J. Mayrhofer, S. Cherevko, *ChemSusChem* **2017**, *10*, 4140.
[96] R. Frydendal, E. A. Paoli, B. P. Knudsen, B. Wickman, P. Malacrida, I. E. L. Stephens, I. Chorkendorff, *ChemElectroChem* **2014**, *1*, 2075.
[97] O. Kasian, S. Geiger, T. Li, J. P. Grote, K. Schweinar, S. Zhang, C. Scheu, D. Raabe, S. Cherevko, B. Gault, K. J. J. Mayrhofer, *Energy Environ. Sci.* **2019**, *12*, 3548.
[98] J. Chen, H. Li, Z. Yu, C. Liu, Z. Yuan, C. Wang, S. Zhao, G. Henkelman, S. Li, L. Wei, Y. Chen, *Adv. Energy Mater.* **2020**, *10*, 2002593.
[99] J. A. Gauthier, C. F. Dickens, L. D. Chen, A. D. Doyle, J. K. Nørskov, *J. Phys. Chem. C* **2017**, *121*, 11455.
[100] Z. Wu, M. Zhang, H. Jiang, C. J. Zhong, Y. Chen, L. Wang, *Phys. Chem. Chem. Phys.* **2017**, *19*, 15444.
[101] Z. P. Wu, B. Miao, E. Hopkins, P. Keonwoo, Y. Chen, H. Jiang, M. Zhang, C. J. Zhong, L. Wang, *J. Phys. Chem. C* **2019**, *123*, 20853.
[102] J. A. Gauthier, S. Ringe, C. F. Dickens, A. J. Garza, A. T. Bell, M. Head-Gordon, J. K. Nørskov, K. Chan, *ACS Catal.* **2019**, *9*, 920.
[103] L. F. Li, Y. F. Li, Z. P. Liu, *ACS Catal.* **2020**, *10*, 2581.
[104] M. A. Hubert, A. M. Patel, A. Gallo, Y. Liu, E. Valle, M. Ben-Naim, J. Sanchez, D. Sokaras, R. Sinclair, J. K. Nørskov, L. A. King, M. Bajdich, T. F. Jaramilo, *ACS Catal.* **2020**, *10*, 12182.

Huabin Zhang received his Ph.D. degree in Physical Chemistry from Fujian Institute of Research on the Structure of Matter, Chinese Academy of Sciences (FJIRSM-CAS). After finishing his post-doc research in Prof. Xiong Wen (David) Lou's group at Nanyang Technological University, Singapore, he joined King Abdullah University of Science and Technology (KAUST) as an assistant professor in January 2021. His research interests focus on advanced catalysis for sustainable energy.

Xiong Wen (David) Lou received his B.Eng. (first class honors) (2002) and M.Eng. (2004) degrees from the National University of Singapore. He obtained his Ph.D. degree in Chemical Engineering from Cornell University in 2008. He is currently the Cheng Tsang Man Chair Professor in Energy at Nanyang Technological University, Singapore. His current research is focused on the design and synthesis of nanostructured materials for different applications in batteries, electrocatalysis, and photocatalysis.